

# Scalable Krylov Subspace Methods for Generalized Mixed Effects Models with Crossed Random Effects

Pascal Kündig<sup>\*†§</sup>      Fabio Sigrist<sup>†\*</sup>

December 19, 2025

## Abstract

Mixed-effects models are widely used to model data with hierarchical grouping structures and high-cardinality categorical predictor variables. However, for high-dimensional crossed random effects, sparse Cholesky decompositions, the current standard approach, can become prohibitively slow. In this work, we present Krylov subspace-based methods that address these computational bottlenecks and analyze them both theoretically and empirically. In particular, we derive new results on the convergence and accuracy of the preconditioned stochastic Lanczos quadrature and conjugate gradient methods for mixed-effects models, and we develop scalable methods for calculating predictive variances. In experiments with simulated and real-world data, the proposed methods yield speedups by factors of up to about 10,000 and are numerically more stable than Cholesky-based computations as implemented in state-of-the-art packages such as `lme4` and `glmmTMB`. Our methodology is available in the open-source C++ software library `GPBoost`, with accompanying high-level Python and R packages.

## 1 Introduction

Mixed effects models are widely used in various scientific disciplines to analyze data with hierarchically grouped structures [Pinheiro and Bates, 2000, McCulloch and Searle, 2004]. High-dimensional crossed random effects occur frequently in practice, for instance, when modeling ratings in recommender systems with categorical grouping variables corresponding to customers and products [Gao and Owen, 2017, Ghosh et al., 2022a, Simchoni and Rosset, 2023] or, in general, when there are high-cardinality categorical predictor variables [Simchoni and Rosset, 2021, Sigrist, 2023b]. However, current standard sparse Cholesky decomposition-based computations can become prohibitively slow for high-dimensional crossed random effects. For instance, the cost of computing Cholesky factors has up to cubic complexity in the dimension of the random effects [Pandolfi et al., 2025].

Various methods have been proposed to overcome this computational bottleneck, including method of moments estimation [Gao and Owen, 2017, 2020], collapsed Gibbs samplers [Papaspiliopoulos et al., 2020, 2023], backfitting algorithms [Ghosh et al., 2022b,a], composite likelihoods [Bellio et al., 2023, Xu et al., 2023], and variational inference [Xu et al., 2023, Goplerud et al., 2025]. Furthermore, the preconditioned conjugate gradient (CG) method [Saad, 2003] with relatively simple diagonal or block-diagonal preconditioners has been applied to solve high-dimensional mixed model equations [Strandén and Lidauer, 1999, 2001, Tsuruta et al., 2001, Taskinen et al., 2017, Garrick et al., 2019, Vandenplas et al., 2018]. Recently, Pandolfi et al. [2025] have analyzed the CG method with diagonal preconditioning for Bayesian generalized linear mixed models (GLMMs). For Gaussian likelihoods and the special case where all random effects have the same variance, Border and Becker [2019] and Cheng et al. [2023] use stochastic Lanczos quadrature (SLQ) [Ubaru et al., 2017] without preconditioning in combination with a shift-invariance property to calculate log-determinants in log-marginal likelihoods. However, without preconditioning, SLQ-approximated log-marginal likelihoods have high variances and

---

<sup>\*</sup>Lucerne University of Applied Sciences and Arts

<sup>†</sup>Seminar for Statistics, ETH Zurich

<sup>‡</sup>University of Basel

<sup>§</sup>Corresponding author: pascal.kuendig@gmail.com

are thus inaccurate; see our theoretical and empirical analyses below. An accurate and scalable method for calculating log-determinants with a theoretical understanding of its convergence properties is thus currently missing. Furthermore, to our knowledge, there exists no scalable method for calculating predictive variances when the number of prediction points is large.

In this article, we introduce Krylov subspace methods for computationally efficient parameter estimation and the calculation of posterior predictive distributions for generalized mixed effects models with Gaussian and non-Gaussian likelihoods. Krylov subspace methods allow for fast computations as they rely on matrix-vector multiplications with sparse matrices, which can be trivially parallelized. We use the preconditioned CG and SLQ methods to solve sparse linear systems and to calculate log-determinants in log-likelihoods, respectively. Gradients of log-marginal likelihoods are calculated using stochastic trace estimation (STE), with almost no computational overhead once marginal likelihoods are computed.

We theoretically and empirically analyze the proposed methods. In particular, we derive novel results on extremal eigenvalues, condition numbers, and thus the convergence behavior of the SLQ method for the symmetric successive over-relaxation (SSOR) and diagonal preconditioners, as well as for the unpreconditioned case. Moreover, we present new results on the effective condition numbers and, hence, on the convergence of the CG method for the SSOR preconditioner, extending the results of [Pandolfi et al. \[2025\]](#) for the diagonal preconditioner. Our theoretical and empirical results show that the SSOR preconditioner yields more accurate SLQ-approximated log-marginal likelihoods and faster convergence of the CG method compared to the diagonal preconditioner and the unpreconditioned case. Furthermore, we introduce scalable and accurate simulation-based methods for calculating predictive variances when the number of prediction points is large. In experiments with simulated and real-world data, the proposed methods yield speedups by factors of up to about 10,000 and are numerically more stable than Cholesky-based computations as implemented in state-of-the-art packages such as `lme4` [[Bates et al., 2015](#)] and `glmmTMB` [[Brooks et al., 2017](#)], while maintaining essentially identical accuracy.

## 2 Preliminaries on Generalized Mixed Effects Models

We assume that the response variable  $y = (y_1, \dots, y_n)^T \in \mathbb{R}^n$  follows a distribution with a density  $p(y|\mu, \xi) = \prod_{i=1}^n p(y_i|\mu_i, \xi)$ , where  $\mu \in \mathbb{R}^n$  are, potentially link function-transformed, parameters, and  $\xi \in \Xi \subset \mathbb{R}^r$  are auxiliary parameters. For instance,  $\mu_i$  and  $\xi$  can be the mean and variance of a Gaussian distribution, the log-mean and the shape parameter of a gamma likelihood, or  $\mu_i$  can be the logit-transformed success probability of a Bernoulli distribution for which there is no additional parameter  $\xi$ . The main parameters of interest  $\mu$  are modeled as the sum of fixed  $F(X)$  and random effects  $Zb$ :

$$\mu = F(X) + Zb, \quad b \sim N(0, \Sigma),$$

where  $X \in \mathbb{R}^{n \times p}$  contains predictor variables. In generalized linear mixed effects models (GLMMs), the fixed effects function is linear,  $F(X) = X\beta$ , but  $F(\cdot)$  can also be modeled using machine learning methods such as regression trees [[Hajjem et al., 2011](#), [Sela and Simonoff, 2012](#), [Fu and Simonoff, 2015](#)], random forests [[Hajjem et al., 2014](#)], tree-boosting [[Sigrist, 2022](#), [2023a](#)], or deep neural networks [[Simchoni and Rosset, 2021](#), [2023](#), [Avanzi et al., 2024](#)]. For notational simplicity, we will denote the parameters of this function  $F(\cdot)$  by  $\beta$ , regardless of whether  $F(\cdot)$  is linear or not. The latent Gaussian variables  $b = (b_1^T, b_2^T, \dots, b_K^T)^T \in \mathbb{R}^m$  consist of  $K$  grouped random effect components  $b_k \in \mathbb{R}^{m_k}$ ,  $k \in \{1, \dots, K\}$ ,  $m = \sum_{k=1}^K m_k$ , and the covariance matrix  $\Sigma \in \mathbb{R}^{m \times m}$  is diagonal and depends on a set of variance parameters  $\theta = \{\sigma_1^2, \sigma_2^2, \dots, \sigma_K^2\}$ :

$$\Sigma = \text{diag}(\underbrace{\sigma_1^2, \dots, \sigma_1^2}_{m_1-\text{times}}, \underbrace{\sigma_2^2, \dots, \sigma_2^2}_{m_2-\text{times}}, \dots, \underbrace{\sigma_K^2, \dots, \sigma_K^2}_{m_K-\text{times}}) \in \mathbb{R}^{m \times m}.$$

In addition,  $Z = (Z_1, Z_2, \dots, Z_K) \in \mathbb{R}^{n \times m}$ ,  $Z_j \in \mathbb{R}^{n \times m_k}$ , is usually a binary incidence matrix that maps the random effects  $b$  to the corresponding observations, but it can also contain predictor variables when modeling random coefficients. We denote such a model as a generalized mixed effects model. Note that the diagonal assumption for  $\Sigma$  is not crucial for the methods presented in the following and could be easily relaxed, e.g., to account for prior correlation among random slopes and intercepts.

## 2.1 Parameter estimation

For parameter estimation, the marginal likelihood  $p(y|\beta, \theta, \xi) = \int p(y|\mu, \xi)p(b|\theta)db$  is typically maximized. For non-Gaussian likelihoods, there is no analytic expression for this marginal likelihood and an approximation has to be used. We use the Laplace approximation since it is computationally efficient and widely used in popular GLMM software libraries such as `lme4` [Bates et al., 2015] and `glmmTMB` [Brooks et al., 2017]. For the Laplace approximation, we further assume that the likelihood  $p(y|\mu, \xi)$  is log-concave and two times continuously differentiable in  $\mu$ . A Laplace approximation to the negative log-marginal likelihood  $-\log(p(y|\beta, \theta, \xi))$  modulo constant terms is given by

$$L^{LA}(y|\beta, \theta, \xi) = -\log p(y|\mu^*, \xi) + \frac{1}{2}b^{*T}\Sigma^{-1}b^* + \frac{1}{2}\log \det(\Sigma) + \frac{1}{2}\log \det(\Sigma^{-1} + Z^TWZ), \quad (1)$$

where  $\mu^* = F(X) + Zb^*$ ,  $b^* = \operatorname{argmax}_b \log p(y|\mu, \xi) - \frac{1}{2}b^T\Sigma^{-1}b$  is the mode of  $p(y|\mu, \xi)p(b|\theta)$ , and  $W \in \mathbb{R}^{n \times n}$  is diagonal with  $W_{ii} = -\frac{\partial^2 \log p(y_i|\mu_i, \xi)}{\partial \mu_i^2} \Big|_{\mu=\mu^*}$ . The mode  $b^*$  is typically found with Newton's method [Rasmussen and Williams, 2006], and one iteration is given by

$$b^{*t+1} = b^{*t} + (Z^TWZ + \Sigma^{-1})^{-1} \left( Z^T \frac{\partial \log p(y|\mu^{*t}, \xi)}{\partial b} - \Sigma^{-1}b^{*t} \right), \quad t = 0, 1, \dots \quad (2)$$

If a first- or second-order optimization method is used for minimizing  $L^{LA}(y|\beta, \theta, \xi)$ , gradients with respect to  $\theta$ ,  $F = F(X) \in \mathbb{R}^n$ , and  $\xi$  are needed. These gradients can be found, e.g., in Sigrist [2023a]. Note that gradients with respect to  $F \in \mathbb{R}^n$  are used, for instance, for GLMMs since  $\frac{\partial L^{LA}(y|\beta, \theta, \xi)}{\partial \beta} = X^T \frac{\partial L^{LA}(y|\beta, \theta, \xi)}{\partial F}$  by the chain rule when  $F(X) = X\beta$ .

For Gaussian likelihoods, we can write

$$y = F(X) + Zb + \epsilon, \quad \epsilon \sim N(0, W^{-1}), \quad W = \frac{1}{\sigma^2} I_n,$$

where  $\sigma^2$  is the error variance and  $I_n \in \mathbb{R}^{n \times n}$  an identity matrix. In this case, the Laplace approximation is exact, and the negative log-marginal likelihood is given by

$$L(y|\beta, \theta, \xi) = \frac{n}{2} \log(2\pi) + \frac{1}{2} \log \det(\Psi) + \frac{1}{2}(y - F(X))^T \Psi^{-1} (y - F(X)), \quad \Psi = Z\Sigma Z^T + W^{-1}. \quad (3)$$

Since the dimension of the random effects  $m$  is usually smaller than the number of observations  $n$  and for sparsity reasons, one uses the Woodbury identity

$$\Psi^{-1} = W - WZ(\Sigma^{-1} + Z^TWZ)^{-1}Z^TW \quad (4)$$

for solving linear systems and the matrix determinant lemma to calculate

$$\log \det(\Psi) = \log \det(\Sigma^{-1} + Z^TWZ) + \log \det(\Sigma) + \log \det(W^{-1}). \quad (5)$$

Gradients, e.g., with respect to the variance parameters are given by

$$\frac{\partial L(y|\beta, \theta, \xi)}{\partial \theta_k} = \frac{1}{2} \operatorname{tr} \left( (\Sigma^{-1} + Z^TWZ)^{-1} \frac{\partial \Sigma^{-1}}{\partial \theta_k} + \Sigma^{-1} \frac{\partial \Sigma}{\partial \theta_k} \right) - \frac{1}{2}(y - F(X))^T \Psi^{-1} \frac{\partial \Psi}{\partial \theta_k} \Psi^{-1} (y - F(X)). \quad (6)$$

The Fisher information  $\mathcal{I} \in \mathbb{R}^{K \times K}$  for  $\theta$ , which can be used for Fisher scoring and for obtaining asymptotic confidence sets, is given by

$$(\mathcal{I})_{kl} = \frac{1}{2} \operatorname{tr} \left( \Psi^{-1} \frac{\partial \Psi}{\partial \theta_k} \Psi^{-1} \frac{\partial \Psi}{\partial \theta_l} \right), \quad 1 \leq k, l \leq K. \quad (7)$$

## 2.2 Prediction

Predictions for latent variables  $\mu_p \in \mathbb{R}^{n_p}$  and response variables  $y_p \in \mathbb{R}^{n_p}$  are made using the posterior predictive distributions  $p(\mu_p|y)$  and  $p(y_p|y)$ , respectively. Note that predictions can be made for random effects  $b$  corresponding to levels present in the training data and new random effects  $b_p \in \mathbb{R}^{m_p}$

that did not occur in the observed data. We denote by  $Z_{po} \in \mathbb{R}^{n_p \times m}$  the matrix that relates the random effects  $b$  from the training data to the prediction points, and by  $Z_{pp} \in \mathbb{R}^{n_p \times m_p}$  the matrix that relates the new random effects  $b_p$  to the prediction points. Using this notation, we have

$$\mu_p = F(X_p) + Z_{po}b + Z_{pp}b_p \in \mathbb{R}^{n_p}, \quad (8)$$

where  $X_p \in \mathbb{R}^{n_p \times p}$  is the predictor variable matrix of the prediction points, and

$$\begin{pmatrix} b \\ \mu_p \end{pmatrix} = \begin{pmatrix} 0 \\ F(X_p) \end{pmatrix} + \begin{pmatrix} (I_m, 0_{m \times m_p}) \\ (Z_{po}, Z_{pp}) \end{pmatrix} \begin{pmatrix} b \\ b_p \end{pmatrix} \sim \mathcal{N} \left( \begin{pmatrix} 0 \\ F(X_p) \end{pmatrix}, \begin{pmatrix} \Sigma & \Sigma Z_{po}^T \\ Z_{po} \Sigma & Z_{po} \Sigma Z_{po}^T + Z_{pp} \Sigma_p Z_{pp}^T \end{pmatrix} \right), \quad (9)$$

where  $(I_m, 0_{m \times m_p}) \in \mathbb{R}^{m \times (m+m_p)}$ ,  $I_m \in \mathbb{R}^{m \times m}$  is an identity matrix,  $0_{m \times m_p} \in \mathbb{R}^{m \times m_p}$  is a matrix of zeros, and  $\Sigma_p = \text{Cov}(b_p)$ . While predictive distributions are less commonly used in classical statistical applications of GLMMs, they are important, for example, in mixed-effects machine learning models [Sigrist, 2022, Simchoni and Rosset, 2023], where probabilistic predictions are required.

For the latent variable  $\mu_p$ , the posterior predictive distribution  $p(\mu_p|y)$  is given by

$$p(\mu_p|y) = \int p(\mu_p|b)p(b|y)db \approx \mathcal{N}(\omega_p, \Omega_p),$$

where

$$\omega_p = F(X_p) + Z_{po}b^*, \quad (10)$$

$$\Omega_p = Z_{po} \Sigma Z_{po}^T + Z_{pp} \Sigma_p Z_{pp}^T - Z_{po} \Sigma Z^T \Psi^{-1} Z \Sigma Z_{po}^T \quad (11)$$

$$= Z_{pp} \Sigma_p Z_{pp}^T + Z_{po} (\Sigma^{-1} + Z^T W Z)^{-1} Z_{po}^T. \quad (12)$$

This can be derived using the fact that a Laplace approximation for  $p(y|\beta, \theta, \xi)$  is equivalent to the approximation  $p(b|y) \approx \mathcal{N}(b^*, (\Sigma^{-1} + Z^T W Z)^{-1})$  since  $p(b|y) = p(y|b)p(b)/p(y)$ , and by applying standard results for conditional distributions of multivariate Gaussian distributions.

For predicting the observable response variables  $y_p$ ,  $y_p|\mu_p \sim p(y_p|\mu_p)$ , an additional integral must be calculated:

$$p(y_p|y) = \int p(y_p|\mu_p)p(\mu_p|y)d\mu_p. \quad (13)$$

This is analytically intractable for most likelihoods but can be approximated using numerical integration or by simulating from  $p(\mu_p|y) \approx \mathcal{N}(\omega_p, \Omega_p)$ . Note that, for notational simplicity, we omit the dependence of  $p(\mu_p|y)$ ,  $p(b|y)$ ,  $p(\mu_p|b)$ ,  $p(y_p|y)$ , and  $p(y_p|\mu_p)$  on  $\beta$ ,  $\theta$ , and  $\xi$ .

For a Gaussian likelihood, the above predictive distributions are exact and available in closed form. The posterior mean in (10) can be equivalently calculated as

$$\omega_p = F(X_p) + Z_{po} \Sigma Z^T \Psi^{-1} (y - F(X)),$$

and  $p(y_p|y)$  is obtained from  $p(\mu_p|y)$  by adding the error variance to the diagonal of  $\Omega_p$ .

### 3 Krylov Subspace Methods for Generalized Mixed Effects Models

Parameter estimation and prediction for models with high-dimensional crossed random effects require the following time-consuming operations all involving operations with the sparse matrix  $\Sigma^{-1} + Z^T W Z \in \mathbb{R}^{m \times m}$ . First, calculating linear solves  $(\Sigma^{-1} + Z^T W Z)u = v$ ,  $v \in \mathbb{R}^m$ , in four tasks: (i) in quadratic forms of log-marginal likelihoods in (3) after applying the Woodbury identity given in (4), (ii) in Newton's method for finding the mode, see (2), (iii) for implicit derivatives of the log-marginal likelihood, see [Sigrist, 2023a, Proposition 2.1], and (iv) for predictive variances  $\text{diag}(\Omega_p)$  given in (11). The latter is particularly challenging as the number of prediction points  $n_p$  is typically large, and  $n_p$  linear systems need to be solved to calculate  $\text{diag}(\Omega_p)$ . Note that predictive variances are required not only for predictive distributions, but also for predictive means of non-Gaussian response variables,

see (13). Second, calculating log-determinants  $\log \det(\Sigma^{-1} + Z^T W Z)$  in (approximate) log-marginal likelihoods  $L(y|\beta, \theta, \xi)$  given in (1) and (5) for non-Gaussian and Gaussian likelihoods, respectively. And third, calculating trace terms such as  $\text{tr}((\Sigma^{-1} + Z^T W Z)^{-1} \frac{\partial(\Sigma^{-1} + Z^T W Z)}{\partial \theta_k})$  for the derivatives of log-determinants and  $\text{tr}(\Psi^{-1} \frac{\partial \Psi}{\partial \theta_k} \Psi^{-1} \frac{\partial \Psi}{\partial \theta_l})$  for entries of the Fisher information. Traditionally, these operations are performed using a Cholesky decomposition of  $\Sigma^{-1} + Z^T W Z$ . In the following, we show how these operations can be done using Krylov subspace methods.

For linear solves with the matrix  $\Sigma^{-1} + Z^T W Z$ , we use the preconditioned conjugate gradient (CG) method, which solves a linear system  $(\Sigma^{-1} + Z^T W Z)u = v$  by iteratively doing matrix-vector multiplications with  $\Sigma^{-1} + Z^T W Z$ . This can be done fast since  $\Sigma^{-1} + Z^T W Z$  is sparse, and convergence is often achieved with  $l \ll m$  iterations. Thus, linear solves can be calculated in  $O(l(m+n))$  time complexity. For completeness, the preconditioned CG algorithm is included in Appendix A.5.

Several techniques have been proposed in the literature to calculate log-determinants of large, symmetric positive definite matrices. Dong et al. [2017] find that stochastic Lanczos quadrature (SLQ) [Ubaru et al., 2017] achieves the highest accuracy and fastest runtime compared to other methods. In this article, we use the SLQ method in combination with the preconditioned CG method to approximate  $\log \det(\Sigma^{-1} + Z^T W Z)$ . Specifically, we first note that

$$\log \det(\Sigma^{-1} + Z^T W Z) = \log \det(P) + \log \det(P^{-\frac{1}{2}}(\Sigma^{-1} + Z^T W Z)P^{-\frac{T}{2}}), \quad (14)$$

where  $P$  is a symmetric positive definite preconditioner matrix; see Section 3.1 for more information on preconditioners. The last term is approximated with the SLQ method [Ubaru et al., 2017] as follows:

$$\log \det(P^{-\frac{1}{2}}(\Sigma^{-1} + Z^T W Z)P^{-\frac{T}{2}}) \approx \frac{n}{t} \sum_{i=1}^t e_1^T \log(\tilde{T}_i) e_1, \quad (15)$$

where  $z_1, \dots, z_t \in \mathbb{R}^m$  are i.i.d. random vectors with  $\mathbb{E}[z_i] = 0$  and  $\mathbb{E}[z_i z_i^T] = P$ ,  $\tilde{Q}_i \tilde{T}_i \tilde{Q}_i^T \approx P^{-\frac{1}{2}}(\Sigma^{-1} + Z^T W Z)P^{-\frac{T}{2}}$  is a partial Lanczos decomposition obtained after  $l$  steps of the Lanczos algorithm with  $P^{-\frac{1}{2}}z_i/\|P^{-\frac{1}{2}}z_i\|_2$  as initial vector,  $\tilde{Q}_i \in \mathbb{R}^{m \times l}$  has orthonormal columns,  $\tilde{T}_i \in \mathbb{R}^{l \times l}$  is tridiagonal, and  $e_1 = (1, 0, \dots, 0)^T$ . In this article, we use Gaussian random vectors  $z_i \sim \mathcal{N}(0, P)$ . Wenger et al. [2022] highlight that a decomposition with a preconditioner as in (14) leads to a reduction in variance. Intuitively, the more accurate the preconditioner  $P \approx (\Sigma^{-1} + Z^T W Z)$ , the smaller  $\log \det(P^{-\frac{1}{2}}(\Sigma^{-1} + Z^T W Z)P^{-\frac{T}{2}})$ , and thus the smaller the variance of its stochastic approximation.

Similarly as in Gardner et al. [2018], we use a technique from Saad [2003] to calculate the partial Lanczos tridiagonal matrices  $\tilde{T}_1, \dots, \tilde{T}_t$  from the coefficients of the preconditioned CG algorithm when solving  $(\Sigma^{-1} + Z^T W Z)^{-1}z_1, \dots, (\Sigma^{-1} + Z^T W Z)^{-1}z_t$   $t$  times; see Appendix A.5. In doing so, we avoid running the Lanczos algorithm, which brings multiple advantages: Numerical instabilities of the Lanczos algorithm due to loss of orthogonality [Saad, 2003] are not an issue, storing  $\tilde{Q}_i$  is not necessary, and the linear solves  $(\Sigma^{-1} + Z^T W Z)^{-1}z_i$  can be reused in stochastic trace estimation (STE) for calculating derivatives of the log-determinant, e.g., as follows:

$$\frac{\partial \log \det(\Sigma^{-1} + Z^T W Z)}{\partial \theta_k} \approx \frac{1}{t} \sum_{i=1}^t ((\Sigma^{-1} + Z^T W Z)^{-1} z_i)^T \frac{\partial(\Sigma^{-1} + Z^T W Z)}{\partial \theta_k} P^{-1} z_i.$$

Gradients can thus be calculated with minimal computational overhead once the likelihood is calculated. In Appendix A.3, we show in detail how to calculate derivatives of log-determinants with respect to  $\theta$ ,  $F$ ,  $b^*$ , and  $\xi$ , using STE and a form of variance reduction with control variates based on the SSOR preconditioner introduced in the next section.

Trace terms of the Fisher information given in (7) can also be approximated with STE as follows:

$$\begin{aligned} \text{tr} \left( \Psi^{-1} \frac{\partial \Psi}{\partial \theta_k} \Psi^{-1} \frac{\partial \Psi}{\partial \theta_l} \right) &= \text{tr} \left( (W - W Z (\Sigma^{-1} + Z^T W Z)^{-1} Z^T W) Z_k Z_k^T \right. \\ &\quad \left. (W - W Z (\Sigma^{-1} + Z^T W Z)^{-1} Z^T W) Z_l Z_l^T \right) \\ &\approx \frac{1}{t} \sum_{i=1}^t \left( (Z_k Z_k^T W - Z_k Z_k^T W Z (\Sigma^{-1} + Z^T W Z)^{-1} Z^T W) z_i \right)^T \\ &\quad (W Z_l Z_l^T - W Z (\Sigma^{-1} + Z^T W Z)^{-1} Z^T W Z_l Z_l^T) z_i, \end{aligned} \quad (16)$$

where we use the Woodbury identity,  $\frac{\partial \Psi}{\partial \theta_k} = Z_k Z_k^T$ , and  $z_i \sim \mathcal{N}(0, I_n)$ . Linear solves  $(\Sigma^{-1} + Z^T W Z)^{-1} Z^T W Z z_i$  and  $(\Sigma^{-1} + Z^T W Z)^{-1} Z^T W Z_l Z_l^T z_i$  in (16) can be computed with the CG method. In experiments, we have found that an alternative STE for the Fisher information given in Appendix A.4 leads to less accurate estimates than the STE in (16) (results not shown).

### 3.1 Preconditioners

Preconditioners reduce the variance of stochastic log-determinant estimators and their derivatives and accelerate the convergence speed of the CG method. The convergence speed and accuracy of the CG and SLQ methods are determined by the spectrum of the preconditioned matrix  $P^{-1/2}(\Sigma^{-1} + Z^T W Z)P^{-T/2}$ ; see Section 4 for more details. To practically use a matrix  $P$  as a preconditioner, we need to construct it, perform linear solves with it, calculate  $\log \det(P)$ , and sample from  $\mathcal{N}(0, P)$  in a computationally efficient manner. In the following, we describe three preconditioners that we analyze in this article. First, we consider the diagonal preconditioner given by

$$P_{\text{Diag}} = \text{diag}((\Sigma^{-1} + Z^T W Z)_{ii}).$$

Furthermore, the “symmetric successive over-relaxation” (SSOR) preconditioner is given by

$$P_{\text{SSOR}} = (L + D)D^{-1}(L + D)^T, \quad (17)$$

where  $D$  is a diagonal matrix with diagonal entries  $(D)_{ii} = (\Sigma^{-1} + Z^T W Z)_{ii}$ , and  $L$  is a strictly lower-triangular matrix with entries  $(L)_{ij} = \mathbf{1}_{\{i>j\}}(\Sigma^{-1} + Z^T W Z)_{ij} = \mathbf{1}_{\{i>j\}}(Z^T W Z)_{ij}$  such that  $\Sigma^{-1} + Z^T W Z = L + L^T + D$ . In addition, the zero fill-in incomplete Cholesky (ZIC) factorization described in Appendix A.6 gives the ZIC preconditioner

$$P_{\text{ZIC}} = \tilde{L} \tilde{L}^T \approx \Sigma^{-1} + Z^T W Z,$$

where  $\tilde{L} \in \mathbb{R}^{m \times m}$  is a sparse lower triangular matrix that has the same sparsity pattern as  $\Sigma^{-1} + Z^T W Z$ . Unfortunately, we sometimes observe breakdowns [Scott and Tuma, 2014], i.e., (clearly) negative numbers in the calculations of square roots.

In Section 4, we theoretically analyze the SSOR and diagonal preconditioners, and in Section 5, we empirically compare the different preconditioners. We have also considered two low-rank preconditioners  $P = \Sigma^{-1} + L_k L_k^T \approx \Sigma^{-1} + Z^T W Z$ , where  $L_k \in \mathbb{R}^{m \times k}$  obtained by (i) using the pivoted Cholesky decomposition [Harbrecht et al., 2012, Gardner et al., 2018] to approximate  $Z^T W Z \approx L_k L_k^T$  and (ii) applying a partial Lanczos algorithm to approximate  $Z^T W Z \approx L_k L_k^T$ . However, both these low-rank preconditioners lead to slow CG convergence and high variances of the SLQ method (results not shown).

### 3.2 Predictive variances

The computational bottleneck for prediction is the calculation of the posterior predictive variances  $\text{diag}(\Omega_p)$  in (11). These are required for predictive distributions of the latent and response variables as well as for predictive means of non-Gaussian response variables. Calculating  $\text{diag}(\Omega_p)$  requires solving  $n_p$  linear equation systems with the matrix  $\Sigma^{-1} + Z^T W Z$ . For high-dimensional crossed random effects and large  $n_p$ , solving these linear systems can thus be computationally prohibitive despite the use of the CG method. We develop and compare three solutions for this: two stochastic estimators relying on the CG method and an approach based on the preconditioned Lanczos algorithm.

#### 3.2.1 Predictive variances using a stochastic estimator for the diagonal of a matrix

Algorithm 1 presents a method for calculating  $\text{diag}(\Omega_p)$  by stochastically approximating  $\text{diag}(Z_{po}(\Sigma^{-1} + Z^T W Z)^{-1} Z_{po}^T)$  in (12). The latter is based on an approach of Bekas et al. [2007] for approximating the diagonal of a matrix  $A \in \mathbb{R}^{n_p \times n_p}$  as  $\text{diag}(A) \approx \frac{1}{s} \sum_{i=1}^s z_i \odot A z_i$ , where  $\odot$  denotes the Hadamard product, and  $z_i \in \mathbb{R}^{n_p}$  are Rademacher random vectors with entries  $\pm 1$ . Linear solves for the stochastic estimator are computed with the preconditioned CG method. We additionally apply variance

reduction in Algorithm 1 by using a control variate based on  $\text{diag}(Z_{po}P^{-1}Z_{po}^T)$ :

$$\begin{aligned} \text{diag}(Z_{po}(\Sigma^{-1} + Z^T W Z)^{-1} Z_{po}^T) &\approx c \odot \text{diag}(Z_{po}P^{-1}Z_{po}^T) \\ &\quad + \frac{1}{t} \sum_{i=1}^t \underbrace{z_i \odot Z_{po}(\Sigma^{-1} + Z^T W Z)^{-1} Z_{po}^T z_i}_{=:h(z_i)} - c \odot \underbrace{z_i \odot Z_{po}P^{-1}Z_{po}^T z_i}_{=:r(z_i)}, \end{aligned}$$

where  $c \in \mathbb{R}^{n_p}$  are the optimal weights for the variance reduction given by  $c_j = \widehat{\text{Cov}}([h(z_i)]_j, [r(z_i)]_j) / \widehat{\text{Var}}([r(z_i)]_j)$ , for  $j = 1, 2, \dots, n_p$ . This variance reduction is important for this stochastic estimator, as otherwise the variance of the stochastic approximation is much larger (results not shown). Algorithm 1 can be trivially parallelized and results in an unbiased and consistent approximation for  $\text{diag}(\Omega_p)$ ; see Appendix A.2 for a proof of Proposition 3.1. Assuming that  $P^{-\frac{1}{2}}Z_{po}^T$  is precomputed,  $P = P^{\frac{1}{2}}P^{\frac{T}{2}}$ , the computational complexity of the algorithm is  $O(sn_p + slm + s\psi)$ , where  $l$  denotes the number of CG iterations,  $s$  the number of simulation iterations, and  $\psi$  the number of non-zero entries in  $P^{-\frac{1}{2}}Z_{po}^T$ .

---

**Algorithm 1** Approximate predictive variances using stochastic estimator for the diagonal of a matrix

---

**Input:** Matrices  $Z_{po}, Z, \Sigma, Z_{pp}, \Sigma_p$ , and  $W$

**Output:** Approximate predictive variances  $\text{diag}(\hat{\Omega}_p)$

- 1: **for**  $i \leftarrow 1$  to  $s$  **do**
- 2:     Sample  $z_i^{(1)} \stackrel{\text{i.i.d.}}{\sim}$  Rademacher,  $z_i^{(1)} \in \mathbb{R}^{n_p}$
- 3:      $z_i^{(2)} \leftarrow Z_{po}(\Sigma^{-1} + Z^T W Z)^{-1} Z_{po}^T z_i^{(1)}$
- 4:      $z_i^{(3)} \leftarrow Z_{po}P^{-1}Z_{po}^T z_i^{(1)}$
- 5: **end for**
- 6:  $c_j \leftarrow \widehat{\text{Cov}}((z_i^{(1)} \odot z_i^{(2)})_j, (z_i^{(1)} \odot z_i^{(3)})_j) / \widehat{\text{Var}}((z_i^{(1)} \odot z_i^{(3)})_j)$ ,  $j = 1, 2, \dots, n_p$ ,  $c = (c_1, \dots, c_{n_p})^T$
- 7:  $\text{diag}(\hat{\Omega}_p) \leftarrow \text{diag}(Z_{pp}\Sigma_p Z_{pp}^T) + c \odot \text{diag}(Z_{po}P^{-1}Z_{po}^T) + \frac{1}{s} \sum_{i=1}^s (z_i^{(1)} \odot z_i^{(2)} - c \odot z_i^{(1)} \odot z_i^{(3)})$

---

**Proposition 3.1.** *Algorithm 1 produces an unbiased and consistent estimator  $\text{diag}(\hat{\Omega}_p)$  for the predictive variances  $\text{diag}(\Omega_p)$  given in (12).*

We have also considered a similar algorithm using the alternative version in (11) for  $\Omega_p$  instead of (12). Specifically,  $\text{diag}(Z_{po}\Sigma Z^T \Psi^{-1} Z \Sigma Z_{po}^T)$  is approximated stochastically with the approach of Bekas et al. [2007] using the Woodbury identity, and all other terms are computed deterministically. However, experiments show that such an algorithm results in less accurate estimates compared to Algorithm 1 (results not shown). Note that Gyger et al. [2024] also use an approach based on Bekas et al. [2007] for predictive covariances in Gaussian process regression.

### 3.2.2 Predictive covariances by simulating from multivariate Gaussian distributions

Algorithm 2 presents an approach that allows for approximating predictive covariances  $\Omega_p$  by sampling from a Gaussian distribution with covariance matrix  $Z_{po}(\Sigma^{-1} + Z^T W Z)^{-1} Z_{po}^T$ . The linear solves  $(\Sigma^{-1} + Z^T W Z)^{-1} z_i^{(3)}$  can be done using the preconditioned CG method and the computational complexity of Algorithm 2 is thus  $O(sn + slm + sn_p)$ . This algorithm can also be trivially parallelized and results in an unbiased and consistent approximation for  $\Omega_p$ ; see Appendix A.2 for a proof of Proposition 3.2. In contrast to Algorithm 1, this method can be used to calculate the entire covariance matrix and not just the variances on the diagonal. Furthermore, Algorithm 2 can be adapted to compute only the predictive variances  $\text{diag}(\Omega_p)$  by summing  $z_i^{(4)} \odot z_i^{(4)}$  in Line 5. We have also considered applying variance reduction to the estimator in Algorithm 2 by using a control variate based on  $Z_{po}P^{-1}Z_{po}^T$ . However, we found that the variance reduction was very small for this estimator and control variate since  $\widehat{\text{Cov}}((z_i^{(4)}(z_i^{(4)})^T)_{jk}, (z_i^{(5)}(z_i^{(5)})^T)_{jk})$ ,  $z_i^{(5)} = Z_{po}P^{-\frac{T}{2}}z_i^{(1)}$  and  $j, k = 1, 2, \dots, n_p$ , is often close to zero. Kündig and Sigrist [2025] has used a similar approach in Gaussian process regression.

**Proposition 3.2.** *Algorithm 2 produces an unbiased and consistent estimator  $\hat{\Omega}_p$  for the predictive covariances  $\Omega_p$  given in (12).*

---

**Algorithm 2** Approximate predictive covariances using simulation

---

**Input:** Matrices  $Z_{po}, Z, \Sigma, Z_{pp}, \Sigma_p$ , and  $W$ 
**Output:** Approximate predictive covariances  $\hat{\Omega}_p$ 

- 1: **for**  $i \leftarrow 1$  to  $s$  **do**
- 2:     Sample  $z_i^{(1)} \stackrel{\text{i.i.d.}}{\sim} \mathcal{N}(0, I_m)$  and  $z_i^{(2)} \stackrel{\text{i.i.d.}}{\sim} \mathcal{N}(0, I_n)$  and set  $z_i^{(3)} \leftarrow \Sigma^{-\frac{1}{2}} z_i^{(1)} + Z^T W^{\frac{1}{2}} z_i^{(2)}$
- 3:      $z_i^{(4)} \leftarrow Z_{po}(\Sigma^{-1} + Z^T W Z)^{-1} z_i^{(3)}$
- 4: **end for**
- 5:  $\hat{\Omega}_p \leftarrow Z_{pp} \Sigma_p Z_{pp}^T + \frac{1}{s} \sum_{i=1}^s z_i^{(4)} (z_i^{(4)})^T$

---

Alternatively, we can use the expression in (11) and approximate  $Z_{po} \Sigma Z^T \Psi^{-1} Z \Sigma Z_{po}^T$  using simulation. Algorithm 3 presents this approach. The linear solve  $\Psi^{-1} z_i^{(3)}$  can be done using the Woodbury identity and the preconditioned CG method. The computational complexity of Algorithm 3 is thus  $O(sn + slm + sn_p)$ . This algorithm also results in an unbiased and consistent approximation for  $\Omega_p$ ; see Appendix A.2 for a proof of Proposition 3.3.

**Proposition 3.3.** *Algorithm 3 produces an unbiased and consistent estimator  $\hat{\Omega}_p$  for the predictive covariances  $\Omega_p$  given in (11).*

---

**Algorithm 3** Approximate predictive covariances using simulation

---

**Input:** Matrices  $Z_{po}, Z, \Sigma, Z_{pp}, \Sigma_p$ , and  $W$ 
**Output:** Approximate predictive covariances  $\hat{\Omega}_p$ 

- 1: **for**  $i \leftarrow 1$  to  $s$  **do**
- 2:     Sample  $z_i^{(1)} \stackrel{\text{i.i.d.}}{\sim} \mathcal{N}(0, I_m)$  and  $z_i^{(2)} \stackrel{\text{i.i.d.}}{\sim} \mathcal{N}(0, I_n)$  and set  $z_i^{(3)} \leftarrow Z \Sigma^{\frac{1}{2}} z_i^{(1)} + W^{-\frac{1}{2}} z_i^{(2)}$
- 3:      $z_i^{(4)} \leftarrow Z_{po} \Sigma Z^T \Psi^{-1} z_i^{(3)}$
- 4: **end for**
- 5:  $\hat{\Omega}_p \leftarrow Z_{po} \Sigma Z_{po}^T + Z_{pp} \Sigma_p Z_{pp}^T - \frac{1}{s} \sum_{i=1}^s z_i^{(4)} (z_i^{(4)})^T$

---

We have also considered another version of such an algorithm. First, applying the Woodbury identity in (11), we obtain

$$Z_{po} \Sigma Z^T \Psi^{-1} Z \Sigma Z_{po}^T = Z_{po} \Sigma Z^T W Z \Sigma Z_{po}^T - Z_{po} \Sigma Z^T W Z (\Sigma^{-1} + Z^T W Z)^{-1} Z^T W Z \Sigma Z_{po}^T. \quad (18)$$

We can then approximate last term in (18) by simulation, and all other terms in (11) are calculated deterministically. However, we found that this algorithm leads to less accurate estimates than Algorithms 2 and 3 (results not shown).

### 3.2.3 Predictive variances using preconditioned Lanczos algorithms

Pleiss et al. [2018] use the Lanczos algorithm to approximate predictive covariance matrices for Gaussian process regression. We adapt and extend this approach for generalized mixed effects models. Specifically, we approximate  $\text{diag}(Z_{po} \Sigma Z^T W Z (\Sigma^{-1} + Z^T W Z)^{-1} Z^T W Z \Sigma Z_{po}^T)$  in (18) by running the Lanczos algorithm with the matrix  $\Sigma^{-1} + Z^T W Z$  using the normalized average of the column vectors of  $Z^T W Z \Sigma Z_{po}^T$  as initial value and approximate  $(\Sigma^{-1} + Z^T W Z)^{-1} Z^T W Z \Sigma Z_{po}^T \approx \tilde{Q} \tilde{T}^{-1} \tilde{Q}^T Z^T W Z \Sigma Z_{po}^T$ , where  $\tilde{Q} \tilde{T} \tilde{Q}^T \approx \Sigma^{-1} + Z^T W Z$  is obtained after  $k$  steps of the Lanczos algorithm,  $\tilde{Q} \in \mathbb{R}^{n \times k}$  has orthonormal columns, and  $\tilde{T} \in \mathbb{R}^{k \times k}$  is tridiagonal.  $\text{diag}(Z_{po} \Sigma Z^T W Z \Sigma Z_{po}^T)$  and the other terms in (11) are deterministically computed, and predictive variances are thus approximated as

$$\begin{aligned} \text{diag}(\hat{\Omega}_p) \approx & \text{diag}(Z_{po} \Sigma Z_{po}^T) + \text{diag}(Z_{pp} \Sigma_p Z_{pp}^T) - \text{diag}(Z_{po} \Sigma Z^T W Z \Sigma Z_{po}^T) \\ & + \text{diag}(Z_{po} \Sigma Z^T W Z \tilde{Q} \tilde{T}^{-1} \tilde{Q}^T Z^T W Z \Sigma Z_{po}^T). \end{aligned} \quad (19)$$

The computation of a rank  $k$  Lanczos approximation requires one matrix-vector multiplication with  $\Sigma^{-1} + Z^T W Z$  in each iteration. Since the Lanczos algorithm suffers from numerical stability issues

due to loss of orthogonality, we use a full reorthogonalization scheme [Wu and Simon, 2000]. Computing the Lanczos approximation then has complexity  $O(k^2m)$ . Furthermore, we consider a similar way of preconditioning as in Kündig and Sigrist [2025] by applying the partial Lanczos algorithm to  $P^{-\frac{1}{2}}(\Sigma^{-1} + Z^T W Z)P^{-\frac{T}{2}} \approx \tilde{Q}\tilde{T}\tilde{Q}$  and correcting for this by using  $P^{-\frac{T}{2}}\tilde{Q}\tilde{T}^{-1}\tilde{Q}P^{-\frac{1}{2}}Z^T W Z \Sigma Z_{po}^T \approx (\Sigma^{-1} + Z^T W Z)^{-1}Z^T W Z \Sigma Z_{po}^T$  as approximation. Note that the Lanczos algorithm requires a symmetric matrix and in contrast to the preconditioned CG method, we need to explicitly calculate a factor  $P^{-\frac{1}{2}}$ , where  $P = P^{\frac{1}{2}}P^{\frac{T}{2}}$ . This is possible for the diagonal, SSOR, and ZIC preconditioners. However, in our experiments, this form of preconditioning does not lead to more accurate predictive variance estimates (results not shown).

### 3.3 Software implementation

The methods presented in this article are implemented in the open-source C++ software library **GPBoost**, with accompanying high-level Python and R packages, see <https://github.com/fabsig/GPBoost>.<sup>\*</sup> For linear algebra calculations, we use the **Eigen** library version 3.4.99 and its sparse matrix algebra operations whenever possible. Multi-processor parallelization is done using **OpenMP**.

## 4 Convergence analysis

In the following, we theoretically analyze the properties of the Krylov subspace methods presented in this article. We denote by  $\lambda_{\min} = \lambda_m \leq \dots \leq \lambda_1 = \lambda_{\max}$  the eigenvalues of a symmetric matrix  $A \in \mathbb{R}^{m \times m}$ . The eigenvalues of the preconditioned matrix  $P^{-1/2}(\Sigma^{-1} + Z^T W Z)P^{-T/2}$  determine the convergence speed and accuracy of the CG and SLQ methods. However, there are important differences among the two methods. It is known that the CG method converges fast if the majority of the eigenvalues are clustered together and an effective condition number  $\kappa_{m-l,k} = \lambda_k / \lambda_{m-l}$  [Van der Sluis and van der Vorst, 1986] is small for small  $k, l \geq 1$ , despite the presence of some outlying small and large eigenvalues; see, e.g., Van der Vorst [2003] and Nishimura and Suchard [2022]. In particular, a large condition number  $\kappa = \lambda_1 / \lambda_m$  is not necessarily a problem for the convergence speed of the CG method. The situation is different for the SLQ method, for which the extremal eigenvalues are important for its convergence properties and accuracy, as described in the following.

The Lanczos algorithm factorizes a symmetric matrix as  $A = QTQ^T$ , where  $Q \in \mathbb{R}^{m \times m}$  is orthonormal, and  $T \in \mathbb{R}^{m \times m}$  is a tridiagonal matrix. This decomposition is computed iteratively, and  $k$  iterations result in an approximation  $A \approx \tilde{Q}\tilde{T}\tilde{Q}^T$ , where  $\tilde{Q} \in \mathbb{R}^{m \times k}$  contains the first  $k$  columns of  $Q$ , and  $\tilde{T} \in \mathbb{R}^{k \times k}$  the corresponding coefficients of  $T$ . In brief, SLQ is based on  $\log \det(A) = \text{tr} \log(A)$ ,  $\log(A) \approx \tilde{Q} \log(\tilde{T}) \tilde{Q}^T$ , and stochastic trace estimation. The logarithm function used in  $\log(A) \approx \tilde{Q} \log(\tilde{T}) \tilde{Q}^T$  is mostly determined by the extremal eigenvalues of  $A = P^{-1/2}(\Sigma^{-1} + Z^T W Z)P^{-T/2}$ . It is known that the Lanczos algorithm approximates the smallest and largest eigenvalues  $\lambda_m$  and  $\lambda_1$  the faster, the smaller  $\lambda_1 - \lambda_m$  and the larger  $(\lambda_{m-1} - \lambda_m)/(\lambda_1 - \lambda_{m-1})$  and  $(\lambda_1 - \lambda_2)/(\lambda_2 - \lambda_m)$ , respectively [Golub and Van Loan, 2013, Theorem 10.1.2, Corollary 10.1.3]. Similar results can also be obtained for other eigenvalues. Moreover, even if the approximation due to the Lanczos algorithm was exact, stochastic trace estimators exhibit increased variance when the spectrum of the matrix  $\log(A)$  is poorly conditioned. The extremal eigenvalues  $\lambda_m$  and  $\lambda_1$  are thus expected to be important for the accuracy of an SLQ-approximated log-determinant. Besides these heuristic arguments, there is convergence theory for SLQ-approximated log-determinants with stochastic error bounds that depend on the condition number  $\kappa = \lambda_1 / \lambda_m$  of  $P^{-1/2}(\Sigma^{-1} + Z^T W Z)P^{-T/2}$ . Below, we restate Theorem 3.2 of Kündig and Sigrist [2025] for mixed effects models.

**Theorem 4.1.** *Let  $\kappa = \lambda_1 / \lambda_m$  denote the condition number of  $P^{-1/2}(\Sigma^{-1} + Z^T W Z)P^{-T/2}$ ,  $C_{mt} = \frac{1}{mt} Q_{\chi_{mt}^2}(1 - \eta/2)$ , where  $Q_{\chi_{mt}^2}(\cdot)$  is the quantile function of a  $\chi^2$ -distribution with  $mt$  degrees of freedom, and  $\hat{\Gamma} = \frac{1}{t} \sum_{i=1}^t \|P^{-\frac{1}{2}} z_i\|_2^2 e_1^T \log(\tilde{T}_i) e_1$  an SLQ approximation. If the SLQ method is run with  $l \geq \frac{\sqrt{3}\kappa}{4} \log\left(\frac{C_{mt} 20 \log(2(\kappa+1)) \sqrt{2\kappa+1}}{\epsilon}\right)$  preconditioned CG steps and  $t \geq \frac{32}{\epsilon^2} \log(\kappa+1)^2 \log\left(\frac{4}{\eta}\right)$  number of random vectors, the following holds for any preconditioner  $P$ :*

$$P(|\hat{\Gamma} - \log \det(P^{-1/2}(\Sigma^{-1} + Z^T W Z)P^{-T/2})| \leq \epsilon m) \geq 1 - \eta, \quad (20)$$

<sup>\*</sup>Krylov subspace methods can be enabled via the parameter `matrix_inversion_method = "iterative"` and the preconditioner is chosen via the parameter `cg_preconditioner_type`.

where  $\epsilon, \eta \in (0, 1)$ .

#### 4.1 Extremal eigenvalues and convergence of the SLQ method

To understand the convergence properties of the SLQ method and to apply Theorem 4.1, we next analyze the extremal eigenvalues  $\lambda_{\min}$  and  $\lambda_{\max}$  and the condition numbers  $\lambda_{\max}/\lambda_{\min}$  of the preconditioned matrices  $P^{-1/2}(\Sigma^{-1} + Z^T W Z)P^{-T/2}$  for the SSOR and diagonal preconditioners as well as the unpreconditioned matrix  $\Sigma^{-1} + Z^T W Z$ . We use the following notation.

**Notation.** We denote by

$$\lambda_{\min}^P = \lambda_m^P \leq \dots \leq \lambda_1^P = \lambda_{\max}^P$$

the eigenvalues of  $P^{-1/2}(\Sigma^{-1} + Z^T W Z)P^{-T/2}$  for a preconditioner  $P$ . The eigenvalues of the unpreconditioned matrix  $\Sigma^{-1} + Z^T W Z$  are denoted by  $\lambda_{\min}^{\text{none}} = \lambda_m^{\text{none}} \leq \dots \leq \lambda_1^{\text{none}} = \lambda_{\max}^{\text{none}}$ . Furthermore, let

$$d_{\max} = \max(Z^T Z) \quad \text{and} \quad d_{\min} = \min(Z^T Z)$$

denote the largest and smallest number of occurrences per random effect, and

$$\sigma_{\min}^2 = \min(\sigma_1^2, \dots, \sigma_K^2) \quad \text{and} \quad \sigma_{\max}^2 = \max(\sigma_1^2, \dots, \sigma_K^2).$$

We call a random effects design “balanced” if every random effect  $(b_k)_j \in \mathbb{R}$ ,  $j = 1, \dots, m_k$ ,  $k = 1, \dots, K$ , occurs exactly  $d$  times, i.e.,  $d = n/m_k = \sum_{i=1}^n (Z_k)_{ij}$  for all  $1 \leq j \leq m_k$  and  $k = 1, \dots, K$ .

In Lemmas 4.1 and 4.2, we first derive bounds for the extremal eigenvalues in the general case including Gaussian and non-Gaussian likelihoods. Proofs of Lemmas 4.1 and 4.2 can be found in Appendix A.1. Based on these results, we derive in Theorem 4.2 upper and lower bounds for the condition numbers if  $K = 2$  and the likelihood is Gaussian. If the random effects design is balanced, the condition numbers for the SSOR and diagonal preconditioners are known exactly. Theorem 4.2 also analyzes and compares these condition numbers asymptotically for large  $d_{\max}$  and  $d$ , i.e., when the matrix  $\Sigma^{-1} + Z^T W Z$  is usually less sparse and preconditioners are thus even more important given that computations per CG iteration are more expensive. Furthermore, in Theorem 4.3, we derive upper bounds for the condition numbers for Bernoulli likelihoods.

**Lemma 4.1.** If  $K = 2$ , the following hold true for the SSOR preconditioner:

$$\lambda_{m_1}^{\text{SSOR}} = \dots = \lambda_1^{\text{SSOR}} = \lambda_{\max}^{\text{SSOR}} = 1, \quad (21)$$

$$1 - \frac{1}{(\min(\Sigma_{ii}^{-1}(Z^T W Z)_{ii}^{-1}) + 1)^2} \leq \lambda_{\min}^{\text{SSOR}} \leq 1 - \frac{1}{(\max(\Sigma_{ii}^{-1}(Z^T W Z)_{ii}^{-1}) + 1)^2}, \quad (22)$$

$$1 - \frac{\max((Z^T W Z)_{ii})^2}{\min((D_1)_{ii}) \min((D_2)_{ii})} \leq \lambda_{\min}^{\text{SSOR}} \leq 1 - \frac{\min((Z^T W Z)_{ii})^2}{\max((D_1)_{ii}) \max((D_2)_{ii})}, \quad (23)$$

where  $D_1 = \text{diag}((\Sigma^{-1} + Z^T W Z)_{ii}) \in \mathbb{R}^{m_1 \times m_1}$  and  $D_2 = \text{diag}((\Sigma^{-1} + Z^T W Z)_{ii}) \in \mathbb{R}^{(m-m_1) \times (m-m_1)}$ .

**Lemma 4.2.** For the diagonal preconditioner  $P_{\text{Diag}} = D$ , it holds that

$$1 + \frac{K-1}{\max(\Sigma_{ii}^{-1}(Z^T W Z)_{ii}^{-1}) + 1} \leq \lambda_{\max}^{\text{Diag}} \leq 1 + \frac{K-1}{\min(\Sigma_{ii}^{-1}(Z^T W Z)_{ii}^{-1}) + 1}, \quad (24)$$

$$\frac{1}{1 + \max(\Sigma_{ii}(Z^T W Z)_{ii})} \leq \lambda_{m+1-k}^{\text{Diag}} \leq \frac{1}{1 + \min(\Sigma_{ii}(Z^T W Z)_{ii})}, \quad k = 1, \dots, K-1. \quad (25)$$

Moreover, the following hold true for the unpreconditioned matrix  $\Sigma^{-1} + Z^T W Z$ :

$$\frac{1}{\max(\Sigma_{ii})} + K \min((Z^T W Z)_{ii}) \leq \lambda_{\max}^{\text{none}} \leq \frac{1}{\min(\Sigma_{ii})} + K \max((Z^T W Z)_{ii}), \quad (26)$$

$$\frac{1}{\max(\Sigma_{ii})} \leq \lambda_{m+1-k}^{\text{none}} \leq \frac{1}{\min(\Sigma_{ii})}, \quad k = 1, \dots, K-1. \quad (27)$$

**Theorem 4.2.** *If  $K = 2$  and the likelihood is Gaussian, it holds that*

$$\frac{1}{1 - \left( \frac{\sigma_{\min}^2 d_{\min}}{\sigma^2 + \sigma_{\min}^2 d_{\min}} \right)^2} \leq \frac{\lambda_{\min}^{\text{SSOR}}}{\lambda_{\min}^{\text{SSOR}}} \leq \frac{1}{1 - \left( \frac{\sigma_{\max}^2 d_{\max}}{\sigma^2 + \sigma_{\max}^2 d_{\max}} \right)^2} = \frac{1}{2} \frac{\sigma_{\max}^2 d_{\max}}{\sigma^2} + \frac{3}{4} + o(1) \quad (d_{\max} \rightarrow \infty), \quad (28)$$

$$2 \frac{\sigma_{\min}^2 d_{\min}}{\sigma^2} + 1 \leq \frac{\lambda_{\max}^{\text{Diag}}}{\lambda_{\min}^{\text{Diag}}} \leq 2 \frac{\sigma_{\max}^2 d_{\max}}{\sigma^2} + 1, \quad (29)$$

$$2 \frac{\sigma_{\min}^2 d_{\min}}{\sigma^2} + \frac{\sigma_{\min}^2}{\sigma_{\max}^2} \leq \frac{\lambda_{\max}^{\text{none}}}{\lambda_{\min}^{\text{none}}} \leq 2 \frac{\sigma_{\max}^2 d_{\max}}{\sigma^2} + \frac{\sigma_{\max}^2}{\sigma_{\min}^2}. \quad (30)$$

If, in addition, the design of the random effects is balanced, the following hold:

$$\frac{\lambda_{\max}^{\text{SSOR}}}{\lambda_{\min}^{\text{SSOR}}} = \frac{1}{1 - \left( \frac{1}{\frac{\sigma^2}{\sigma_1^2 d} + 1} \right) \left( \frac{1}{\frac{\sigma^2}{\sigma_2^2 d} + 1} \right)} = \frac{\sigma_1^2 \sigma_2^2}{\sigma^2 (\sigma_1^2 + \sigma_2^2)} d + 1 + o(1) \quad (d \rightarrow \infty), \quad (31)$$

$$\frac{\lambda_{\max}^{\text{Diag}}}{\lambda_{\min}^{\text{Diag}}} = \frac{\sqrt{\left( \frac{\sigma^2}{\sigma_1^2 d} + 1 \right) \left( \frac{\sigma^2}{\sigma_2^2 d} + 1 \right) + 1}}{\sqrt{\left( \frac{\sigma^2}{\sigma_1^2 d} + 1 \right) \left( \frac{\sigma^2}{\sigma_2^2 d} + 1 \right) - 1}} = \frac{4 \sigma_1^2 \sigma_2^2}{\sigma^2 (\sigma_1^2 + \sigma_2^2)} d + 1 + o(1) \quad (d \rightarrow \infty). \quad (32)$$

A proof of Theorem 4.2 can be found in Appendix A.1. This theorem has the following implications. First, Theorem 4.2 shows that the condition numbers  $\lambda_{\max}^{\text{P}}/\lambda_{\min}^{\text{P}}$  of the SSOR and diagonal preconditioners as well as the unpreconditioned matrix do not directly depend on neither the sample size  $n$  nor the dimension of the random effects  $m$  but rather only on (i) the number of occurrences per random effect ( $(Z^T Z)_{ii}$  ( $= d = n/m_1 = n/m_2$  when having a balanced design)) and (ii) the signal-to-noise ratios  $\sigma_k^2/\sigma^2$  (and  $\sigma_{\max}^2/\sigma_{\min}^2$  when no preconditioning is used). Specifically, we find that the condition numbers are increasing in the number of repeated occurrences per random effect and the signal-to-noise ratios. Concerning the former, the theorem shows that the condition numbers  $\lambda_{\max}^{\text{P}}/\lambda_{\min}^{\text{P}}$  of the SSOR and diagonal preconditioners both grow asymptotically linearly in  $d$  when having a balanced random effects design. However,  $\lambda_{\max}^{\text{Diag}}/\lambda_{\min}^{\text{Diag}}$  asymptotically grows four times faster in  $d$  than  $\lambda_{\max}^{\text{SSOR}}/\lambda_{\min}^{\text{SSOR}}$ ; see (31) and (32). Regarding the signal-to-noise ratios, similar arguments as in the derivations of the asymptotic results in (31) and (32) can be made that  $\lambda_{\max}^{\text{SSOR}}/\lambda_{\min}^{\text{SSOR}}$  and  $\lambda_{\max}^{\text{Diag}}/\lambda_{\min}^{\text{Diag}}$  both have linear asymptotes in the “average” signal-to-noise ratio  $2\sigma_1^2 \sigma_2^2 / (\sigma^2 (\sigma_1^2 + \sigma_2^2))$ . Again,  $\lambda_{\max}^{\text{SSOR}}/\lambda_{\min}^{\text{SSOR}}$  grows four times slower in this signal-to-noise ratio compared to  $\lambda_{\max}^{\text{Diag}}/\lambda_{\min}^{\text{Diag}}$ . Analogous arguments concerning  $d_{\max}$  and the signal-to-noise ratio can be made for the upper bounds of the condition numbers for general, non-balanced designs.

Moreover, Theorem 4.2 implies

$$\lambda_{\max}^{\text{SSOR}} < \lambda_{\max}^{\text{Diag}} \quad \text{and} \quad \lambda_{\min}^{\text{SSOR}} > \lambda_{\min}^{\text{Diag}}.$$

This holds for all random effects designs and parameter choices. For the balanced design, we can additionally obtain an explicit expression for the condition number of the unpreconditioned matrix  $\Sigma^{-1} + Z^T W Z$  if the two random effects have equal variances since the inequalities in (30) then become equalities. In this special case, the condition numbers of the unpreconditioned and the diagonal-preconditioned matrix are equal and given by  $2\sigma_1^2 d / \sigma^2 + 1$ .

Next, in Theorem 4.3, we derive upper bounds for the condition numbers of  $P^{-1/2}(\Sigma^{-1} + Z^T W Z)P^{-T/2}$  for a Bernoulli likelihood with logit and probit links used in binary classification. Similarly as for a Gaussian likelihood, the upper bound for the condition number  $\lambda_{\max}^{\text{SSOR}}/\lambda_{\min}^{\text{SSOR}}$  of the SSOR preconditioner given in (33) is smaller and grows four times slower in both (i) the maximal number of repeated random effects occurrences  $d_{\max}$  and (ii) the maximal random effects variance  $\sigma_{\max}^2$  compared to the diagonal preconditioner and the unpreconditioned matrix given in (34) and (35), respectively. A proof of Theorem 4.3 can be found in Appendix A.1.

**Theorem 4.3.** *If  $K = 2$  and the likelihood is Bernoulli with a logit or probit link, it holds that*

$$\frac{\lambda_{\max}^{\text{SSOR}}}{\lambda_{\min}^{\text{SSOR}}} \leq \frac{1}{1 - \left( \frac{\sigma_{\max}^2 d_{\max} C}{1 + \sigma_{\max}^2 d_{\max} C} \right)^2} = \frac{1}{2} \sigma_{\max}^2 d_{\max} C + \frac{3}{4} + o(1) \quad (d_{\max} \rightarrow \infty), \quad (33)$$

$$\frac{\lambda_{\max}^{\text{Diag}}}{\lambda_{\min}^{\text{Diag}}} \leq 2\sigma_{\max}^2 d_{\max} C + 1, \quad (34)$$

$$\frac{\lambda_{\max}^{\text{none}}}{\lambda_{\min}^{\text{none}}} \leq 2\sigma_{\max}^2 d_{\max} C + \frac{\sigma_{\max}^2}{\sigma_{\min}^2}, \quad (35)$$

where  $C$  equals 0.25 and 1 for a logit and a probit link, respectively.

In summary, the results in Theorems 4.1, 4.2, and 4.3, imply that the SSOR preconditioner is expected to yield more accurate SLQ-approximated log-determinants compared to applying no preconditioning and to the diagonal preconditioner for both Gaussian and non-Gaussian likelihoods. These findings are empirically confirmed in the experiments in Section 5.

## 4.2 Effective condition numbers and convergence of the CG method

Under additional assumptions on the random effects design, we derive in Theorem 4.4 a stochastic upper bound for the effective condition number  $\kappa_{m-1,1}^{\text{SSOR}} = \lambda_1^{\text{SSOR}} / \lambda_{m-1}^{\text{SSOR}}$  of the SSOR preconditioner obtained after removing the smallest eigenvalue. Note that the assumptions of Theorem 4.4, which are the same as in Pandolfi et al. [2025, Section 5.4.1], imply that the random effects design is balanced in the sense that every random effect occurs  $d_k$  times for  $k = 1, 2$ ,  $d_k = n/m_k = \sum_{i=1}^n (Z_k)_{ij}$ ,  $\forall 1 \leq j \leq m_k$ , and that all pairs of elements of  $b_1 \in \mathbb{R}^{m_1}$  and  $b_2 \in \mathbb{R}^{m_2}$  co-occur at most once in all observations, i.e.,  $Z_2^T Z_1 \in \{0, 1\}^{m_2 \times m_1}$ . This theorem shows that  $\kappa_{m-1,1}^{\text{SSOR}}$  decreases fast to one as the number of occurrences per random effect  $d_k$  increases. Consequently, the preconditioned CG method is expected to converge faster for larger  $d_k$ ; see the discussion at the beginning of Section 4.

**Theorem 4.4.** *If  $K = 2$ , the likelihood is Gaussian, and  $\begin{pmatrix} 0 & Z_1^T Z_2 \\ Z_2^T Z_1 & 0 \end{pmatrix} \in \{0, 1\}^{m \times m}$  is an adjacency matrix of a random bipartite, biregular graph with uniform distribution over all bipartite, biregular graphs, the following holds:*

$$\kappa_{m-1,1}^{\text{SSOR}} = \frac{\lambda_1^{\text{SSOR}}}{\lambda_{m-1}^{\text{SSOR}}} \leq \frac{1}{1 - \left( \frac{1}{d_1} + \frac{1}{d_2} + \frac{2}{\sqrt{d_1 d_2}} \right) - \epsilon_m} \quad (36)$$

asymptotically almost surely with  $\epsilon_m \rightarrow 0$  as  $m \rightarrow \infty$ , where  $d_k = \frac{n}{m_k}$  for  $k = 1, 2$ .

A proof of Theorem 4.4 can be found in Appendix A.1. Pandolfi et al. [2025, Theorem 4] derive a similar result for the diagonal preconditioner. However, the upper bound for the effective condition number  $\kappa_{m-1,1}^{\text{SSOR}}$  of the SSOR-preconditioned matrix given in (36) decreases faster than the corresponding upper bound for the diagonal preconditioner which is given by

$$\kappa_{m-1,2}^{\text{Diag}} = \frac{\lambda_2^{\text{Diag}}}{\lambda_{m-1}^{\text{Diag}}} \leq \frac{1 + \frac{1}{\sqrt{d_1}} + \frac{1}{\sqrt{d_2}} + \epsilon_m}{1 - \left( \frac{1}{\sqrt{d_1}} + \frac{1}{\sqrt{d_2}} \right) - \epsilon_m}. \quad (37)$$

To make this explicit, for simplicity we consider the case where  $m_1 = m_2$  in Corollary 4.1. This corollary shows that the effective condition number  $\kappa_{m-1,1}^{\text{SSOR}}$  of the SSOR-preconditioned matrix essentially decreases with a rate of  $4/d$ ,  $d = n/m_1 = n/m_2$ , up to higher-order terms. In contrast, the effective condition number  $\kappa_{m-1,2}^{\text{Diag}}$  of the diagonal preconditioner decreases with a slower rate of  $4/\sqrt{d}$ , again up to higher-order terms. Based on these results, we expect the SSOR preconditioner to lead to faster convergence for the CG method compared to the diagonal preconditioner. A proof of Corollary 4.1 can be found in Appendix A.1. Note that the random effects model used in Pandolfi et al. [2025] contains a random intercept term, which we do not include, and they derive their result for  $\kappa_{m-2,3}^{\text{Diag}}$  instead of  $\kappa_{m-1,2}^{\text{Diag}}$ . However, in Theorem A.2 in Appendix A.1, we show that the result in (37) analogously holds true for the model without a random intercept used in this article.

**Corollary 4.1.** *If  $K = 2$ , the likelihood is Gaussian,  $m_1 = m_2$ , and  $\begin{pmatrix} 0 & Z_1^T Z_2 \\ Z_2^T Z_1 & 0 \end{pmatrix} \in \{0, 1\}^{m \times m}$  is an adjacency matrix of a bipartite, biregular random graph with uniform distribution over all bipartite, biregular random graphs, the following hold:*

$$\kappa_{m-1,1}^{SSOR} = \frac{\lambda_1^{SSOR}}{\lambda_{m-1}^{SSOR}} \leq \frac{1}{1 - \frac{4}{d} - \epsilon_m} = 1 + \frac{4}{d} + \epsilon_m + O\left(\frac{1}{d^2}, \epsilon_m^2, \frac{\epsilon_m}{d}\right), \quad (38)$$

$$\kappa_{m-1,2}^{Diag} = \frac{\lambda_2^{Diag}}{\lambda_{m-1}^{Diag}} \leq \frac{1 + \frac{2}{\sqrt{d}} + \epsilon'_m}{1 - \frac{2}{\sqrt{d}} - \epsilon'_m} = 1 + \frac{4}{\sqrt{d}} + \epsilon'_m + O\left(\frac{1}{d}, \epsilon'_m^2, \frac{\epsilon'_m}{\sqrt{d}}\right) \quad (39)$$

asymptotically almost surely with  $\epsilon_m \rightarrow 0$  and  $\epsilon'_m \rightarrow 0$  as  $m \rightarrow \infty$ , where  $d = n/m_1 = n/m_2$ .

## 5 Experiments using simulated data

In the following, we conduct experiments using simulated data. We compare the different preconditioners and methods for calculating predictive variances. Furthermore, we analyze our proposed methods concerning the accuracy and runtime for parameter estimation and prediction. Krylov subspace methods are compared to computations relying on sparse Cholesky decompositions. Note, however, that Cholesky decompositions also do not necessarily yield exact results since round-off errors can accumulate when using finite precision arithmetic. Code to reproduce the simulated and the real-world data experiments of this article is available at <https://github.com/pkuendig/KrylovGMMS>.

### 5.1 Experimental setting

We simulate data from a model with two crossed random effect components. Unless stated otherwise, we use a balanced random effects design, i.e., each random effect  $b_{k,j}$ ,  $j = 1, \dots, m_k$ ,  $k = 1, 2$ , occurs the same number of times,  $\sum_{i=1}^n (Z_1)_{ij} = \sum_{i=1}^n (Z_2)_{ij} = n/m_1 = n/m_2$ , both random effect components  $b_1$  and  $b_2$  have the same dimension  $m_1 = m_2$ , the crossing structure between the two random effect components is random, and the random effects variances are  $\sigma_1^2 = \sigma_2^2 = 0.25$ . A random crossing structure is generated by generating incidence matrices  $Z_k \in \{0, 1\}^{n \times m_k}$  as follows. We first assign exactly  $n/m_k$  ones to column  $j$  in consecutive rows,  $(Z_k)_{ij} = 1$  for  $i = (j-1)n/m_k + 1, \dots, jn/m_k$ ,  $j = 1, \dots, m_k$ , and zero otherwise, and we randomly permute the rows of  $Z_2$ . We consider various sample sizes  $n$  and dimensions  $m$  of the random effects as described in the subsections below. The response variable  $y$  follows either a Gaussian likelihood with error variance  $\sigma^2 = 0.25$  or a Bernoulli likelihood with a logit link function. We additionally conduct experiments for less regular unbalanced designs, unequal dimensions of the random effect components ( $m_1 \neq m_2$ ), and other signal-to-noise ratios. See the subsections below for more information. For the experiments regarding the accuracy and runtimes of parameter estimation and prediction in Sections 5.5 and 5.4, we include a fixed effects linear predictor term with five covariates and an intercept. The regression coefficients are all set to one except for the intercept, which is set to zero, and the covariates are sampled from a normal distribution with mean zero and variance chosen such that the fixed and random effects have equal variance.

For analyzing prediction accuracy, the data is randomly split into training and test data sets. We measure both the accuracy of point and probabilistic predictions for the test random effects  $\tilde{b}_p = Z_{po}b + Z_{pp}b_p$ ; see (8). Point predictions in the form of predictive means are evaluated using the root mean squared error (RMSE), and for probabilistic predictions, we use the log score (LS)  $-\frac{1}{n_p} \sum_{i=1}^{n_p} \log(\mathcal{N}((\tilde{b}_p)_i; \omega_{p,i}, (\Omega_p)_{ii}))$ , where  $\omega_{p,i}$  and  $(\Omega_p)_{ii}$  are the predictive latent means and variances for the random effect  $(\tilde{b}_p)_i$  of test observation  $i$ , and  $\mathcal{N}((\tilde{b}_p)_i; \omega_{p,i}, (\Omega_p)_{ii})$  denotes a Gaussian density evaluated at  $(\tilde{b}_p)_i$ . We also measure the runtime in seconds.

All calculations are done on a laptop with an Intel i7-12800H processor and 32 GB of random-access memory. We use the **GPBoost** library version 1.6.4 for Krylov subspace and Cholesky decomposition-based methods denoted as ‘Krylov (GPBoost)’ and ‘Cholesky (GPBoost)’, respectively. Cholesky-based calculations are additionally done with the **R** packages **lme4** version 1.1-35.5 and **g1mmTMB** version 1.1.10. For Gaussian likelihoods, parameter estimation is done by minimizing the negative log-marginal likelihood. For non-Gaussian likelihoods, all implementations use the Laplace approximation. For parameter estimation, we set the initial values for all models to the default values used by **GPBoost**.

Besides the above-mentioned points, the default options of the packages are used, including package-specific internal optimizers.

For the Krylov subspace methods, if not stated otherwise, we use the SSOR preconditioner and  $t = 50$  random vectors for STE and SLQ. For the CG algorithm, we use a convergence tolerance of  $10^{-2}$  for calculating marginal likelihoods and gradients and a tolerance of  $10^{-3}$  for predictive variances. Unless stated otherwise, we use Algorithm 1 and  $s = 1000$  samples for calculating predictive variances. Further, we adopt a sample average approximation approach [Kim et al., 2015] when maximizing the marginal likelihood.

## 5.2 Preconditioner comparison

We compare the preconditioners introduced in Section 3.1 with regard to the accuracy and runtimes for approximating log-marginal likelihoods. We use a total number of  $m = 100,000$  random effects and a sample size of  $n = 1,000,000$ . These dimensions are approximately the largest such that Cholesky-based computations can be run in a reasonable amount of time (approx. four hours for one likelihood evaluation). Furthermore, we use both a balanced random effects design as described in Section 5.1 and a less regular unbalanced design. The latter is generated as described in Appendix A.7. The calculation of the marginal likelihoods is done at the data-generating parameters and repeated 100 times with different random vectors for the SLQ method.

First, we analyze how the accuracy and runtimes depend on the number of random vectors  $t$  in the SLQ method for a Gaussian likelihood. Figure 1 reports standard deviations of the stochastic estimates and average wall-clock times for the different preconditioners for both the balanced and unbalanced random effects designs. The figure also reports the number of iterations (bottom row, right axis) of the CG method used for calculating the quadratic form in the log-marginal likelihood. The wall-clock time and negative log-marginal likelihood when using a Cholesky decomposition are annotated in the plot. We first observe that the SSOR and ZIC preconditioners yield the most accurate log-marginal likelihood approximations. Compared to the diagonal preconditioner and the unpreconditioned SLQ method, the SSOR and ZIC preconditioners yield standard deviations that are approximately one order of magnitude lower for both random effects designs. This observation is consistent with the theoretical results presented in Section 4. Furthermore, as expected from theory, the diagonal preconditioner does not give any variance reduction for the balanced design, but for the unbalanced design, we observe smaller standard deviations compared to the unpreconditioned CG method. The runtimes and the number of CG iterations are similar for all preconditioners and also without preconditioning for the balanced design. In contrast, for the unbalanced design, all preconditioners substantially reduce the runtimes and numbers of CG iterations. In line with the convergence theory in Section 4, the diagonal preconditioner has a slightly higher number of CG iterations and runtimes compared to the SSOR preconditioner, but the differences are small. Note that the SSOR preconditioner has a higher “overhead” per CG iteration than the diagonal preconditioner since additional sparse triangular solves are done for the SSOR preconditioner. Finally, we observe that the Krylov subspace-based methods are much faster than Cholesky-based calculations. For instance, when using  $t = 50$  random vectors, they result in a speedup of approximately four orders of magnitude. Note that all preconditioners yield unbiased SLQ-approximated log-marginal likelihoods. To empirically verify this, we additionally report in Figure 8 in Appendix A.8 histograms of log-marginal likelihoods.

In Figures 9 and 10 in Appendix A.8, we report analogous results when the likelihood is Bernoulli with a logit link function and all other settings are identical. We find qualitatively very similar results as in the Gaussian setting. In particular, Krylov subspace-based methods are approximately 50,000 times faster than Cholesky-based computations. The SSOR and ZIC preconditioners yield substantially more accurate log-marginal likelihood approximations than the diagonal preconditioner and the unpreconditioned case. Next, in Figure 11 in Appendix A.8, we present additional results when having a higher signal-to-noise ratio obtained by using a lower error variance  $\sigma^2 = 0.05$  for a Gaussian likelihood. The results are again qualitatively similar to the ones of the lower signal-to-noise ratio. We further analyze the impact of the irregularity of the random effects design. For this, we vary the size parameter  $r$  in the unbalanced design generation approach explained in Appendix A.7. The results are reported in the left column of Figure 12 in Appendix A.8. We find that the runtime of the unpreconditioned CG method increases with increasing irregularity, whereas the runtimes remain constant for the preconditioned CG method for all preconditioners. The accuracy of the SLQ method is only marginally affected by the irregularity of the design with and without preconditioning. In the

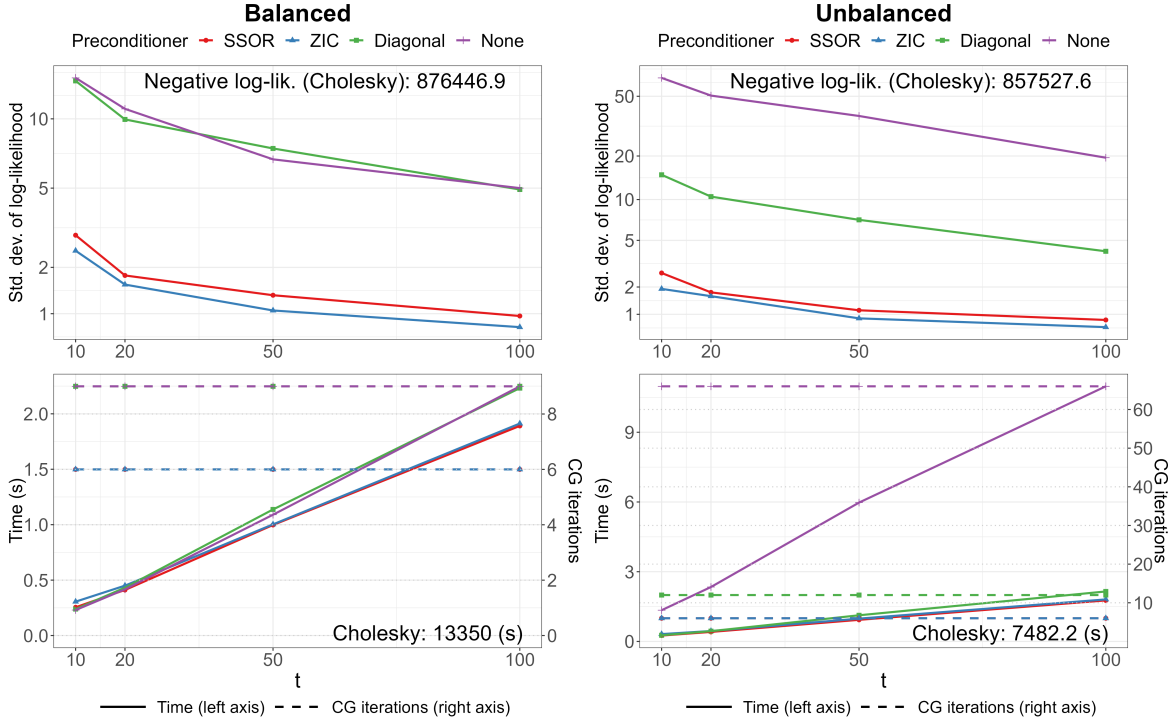


Figure 1: Accuracy (in standard deviations; top row), wall-clock time (in seconds; bottom row, left axis), and number of CG iterations (bottom row, right axis) for different preconditioners and varying numbers of random vectors  $t$  in the SLQ method for calculating log-marginal likelihoods for a Gaussian likelihood and balanced and unbalanced random effects designs.

right column of Figure 12 in Appendix A.8, we also report results when varying the random effects dimension  $m$ . An unbalanced design and a constant ratio  $n/m = 10$  (as above) is used for this experiment. We find that there is a small increase in the variance of the SLQ method, the numbers of CG iterations are essentially constant, but the runtimes of the CG method increases due to a higher computational complexity per CG iteration when  $m$  increases.

### 5.3 Comparing methods for predictive variances

Next, we compare the accuracy of the different methods for calculating predictive variances, as introduced in Section 3.2, using simulated data with  $n = n_p = 100,000$  training and test points and a total of  $m + m_p = 10,000$  group levels. The response variable follows a Gaussian likelihood, and we calculate the RMSE of the approximate predictive variances to the “exact” Cholesky-based predictive variances. We also measure the runtime for prediction, which includes the calculation of the latent predictive means and variances. Predictive distributions are calculated at the data-generating variance parameters.

Figure 2 visualizes the accuracy (RMSE) versus the wall-clock time for different numbers of random vectors  $s$  for the stochastic methods and different ranks  $k$  for the Lanczos-based approximation. For the former, we average the results over 100 independent repetitions for every  $s$  and add confidence intervals for the RMSE obtained as  $\pm 2 \times$  standard errors (not visible since they are very small). The runtime of Cholesky-based calculations is annotated in the plot. By far the most accurate predictive variances for a given runtime are obtained with the simulation-based Algorithm 1. For instance, for  $s = 200$ , predictive variances are very accurate with an RMSE of approximately  $2.6 \times 10^{-4}$ , and the runtime is more than 100 times faster compared to Cholesky-based calculations. Algorithm 2 achieves the second highest prediction accuracy for a given runtime, and Algorithm 3 is considerably slower and less accurate. Finally, Lanczos-based approximations are very inaccurate and the RMSE decreases only very slowly with increasing rank  $k$ .

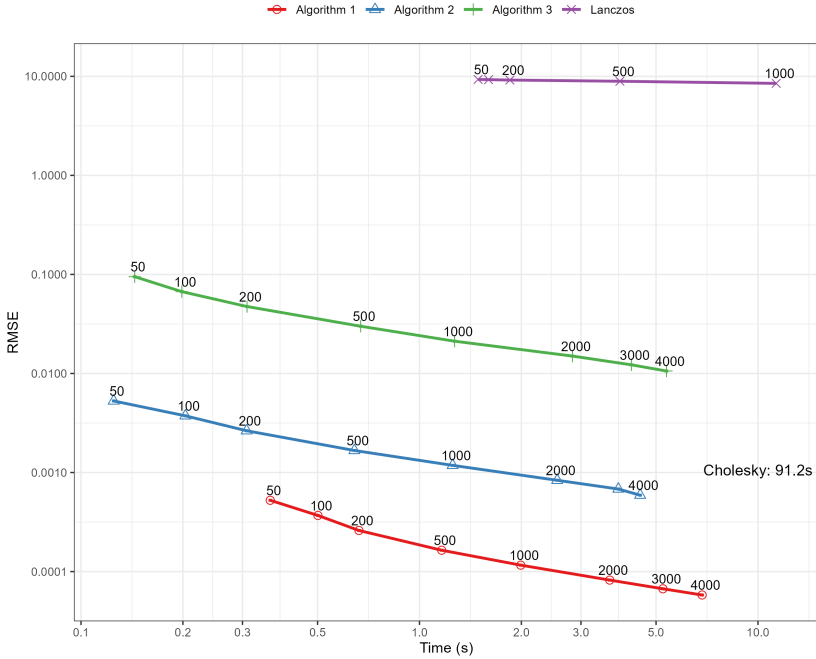


Figure 2: Accuracy-runtime comparison of different methods for predictive variances. The number of random vectors  $s$  and the Lanczos rank  $k$  are annotated in the plot.

#### 5.4 Runtime comparison for parameter estimation

In this subsection, we compare the runtime for parameter estimation when using Krylov subspace methods and Cholesky-based calculations with the `GPBoost`, `lme4`, and `glmmTMB` packages. We consider different dimensions of the random effects ranging from  $m = 1,000$  up to  $m = 1,000,000$  and  $n = 10m$  using the setting described in Section 5.1. In particular, we use two crossed random effect components and include five covariates plus an intercept in a linear predictor. Figure 3 shows the wall-clock time in seconds versus the number of random effects  $m$ . Krylov subspace methods achieve the fastest runtime for all  $m$ . For instance, for  $m = 20,000$  and a Gaussian likelihood, Krylov subspace methods are approximately three orders of magnitudes faster than Cholesky-based computations when using the `GPBoost` package. For a Gaussian likelihood, `glmmTMB` is approximately four orders of magnitudes slower than the Krylov subspace methods implemented in `GPBoost`, and `lme4` is approximately four orders of magnitudes slower than the Krylov subspace methods for a Bernoulli likelihood. In general, estimation takes the longest with `glmmTMB` for Gaussian likelihoods, and for Bernoulli likelihoods, estimation takes the longest with `lme4`.

In Figure 13 in Appendix A.9, we additionally compare the runtime for parameter estimation for a random effects design with  $m_2 = 2$ . Cholesky-based computations are faster compared to the case  $m_1 = m_2$  due to the increased sparsity in  $Z^T W Z$ , but Krylov subspace methods again clearly achieve the fastest runtime for all  $m$ . For instance, they are three orders of magnitude faster than Cholesky-based computations when using `GPBoost` for  $m = 50,000$  and a Gaussian likelihood.

#### 5.5 Accuracy of parameter estimation and predictive distributions

In the following, we analyze the properties of the variance parameter and linear regression coefficient estimates and the accuracy of predictive distributions for Gaussian and Bernoulli likelihoods when using Krylov-subspace methods. As mentioned in Section 5.1, we include five covariates plus an intercept in a linear predictor. We set the total number of training and prediction random effects to  $m + m_p = 4,000$  and simulate  $n = n_p = 40,000$  training and test points. This is roughly the largest number of group levels such that we can run calculations with the `glmmTMB` and `lme4` packages in a reasonable amount of time. We perform 100 simulation repetitions, and prediction is done using estimated parameters. For Bernoulli likelihoods, repeating the estimation 100 times with `lme4` leads to very long runtimes;

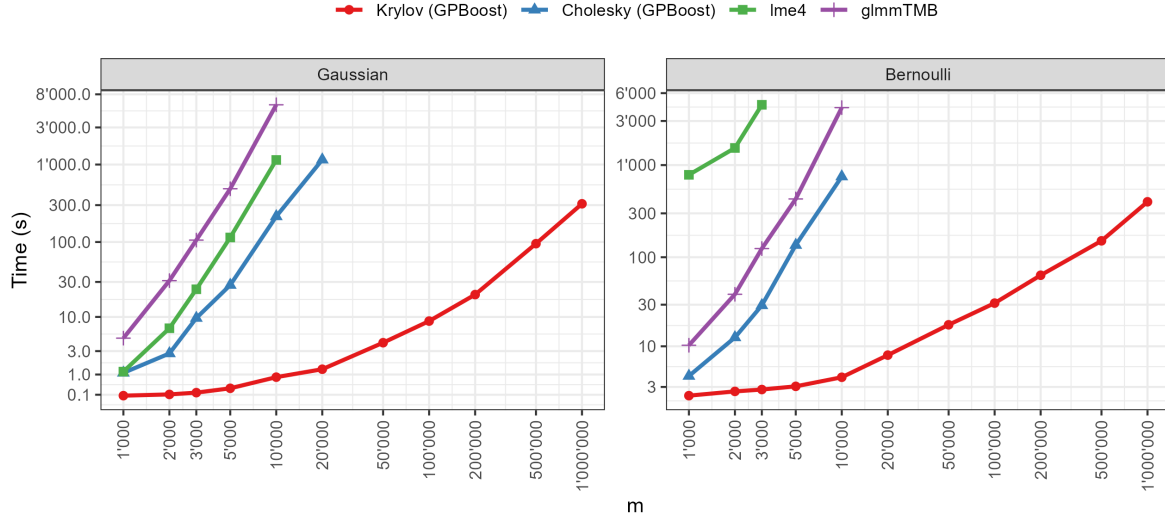


Figure 3: Average wall clock times (s) for parameter estimation and different  $m$ . Simulated data follows either a Gaussian or a Bernoulli likelihood.

see also Section 5.4. Therefore, we do not report estimates and prediction accuracy for this case.

Figure 4 visualizes the estimates for the variance parameters. The RMSE and bias of the variance and regression coefficient estimates are additionally reported in Appendix A.9 in Tables 2 and 3 for Gaussian and Bernoulli likelihoods, respectively. We observe virtually no differences among the estimates obtained using Krylov subspace methods and Cholesky-based computations with the **GPBoost**, **lme4**, and **glmmTMB** packages. Note that the variance parameter estimates for Bernoulli likelihoods are slightly downward biased due to the Laplace approximation and the moderate sample size.

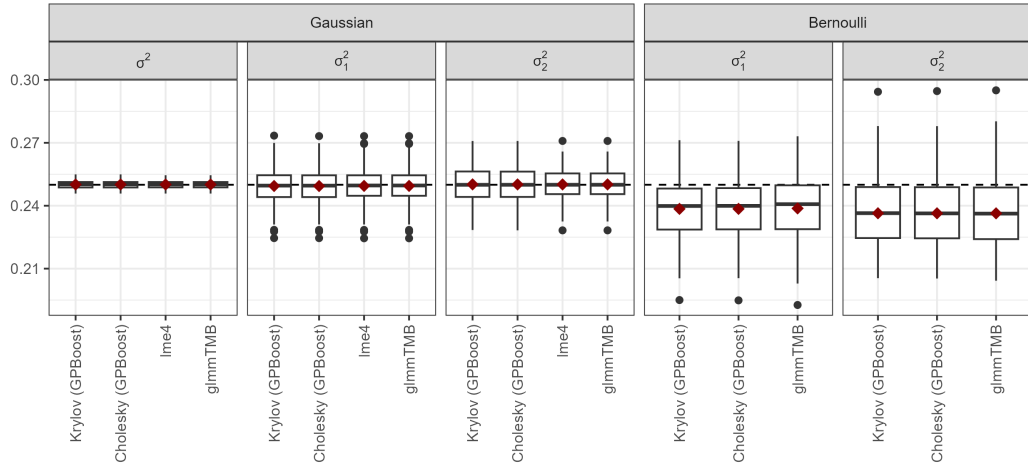


Figure 4: Estimated variance parameters. The red rhombi represent means. The dashed lines indicate the true values. For the Bernoulli likelihood, the estimates for **lme4** are not computed due to excessively long runtimes.

Next, Figure 5 shows the RMSE for predictive means and the log score for predictive distributions. The average RMSE and the average log score with the corresponding standard errors are reported in Appendix A.9 in Tables 4 and 5 for Gaussian and Bernoulli likelihoods, respectively. Log scores are only reported for Krylov subspace methods and Cholesky-based computations from the **GPBoost** package since the calculation of predictive variances is not supported for **lme4** and leads to very long runtimes for **glmmTMB**. We observe that the predictions obtained with the Cholesky decomposition and

the Krylov subspace methods have virtually the same accuracy in terms of both the RMSE and the log score.

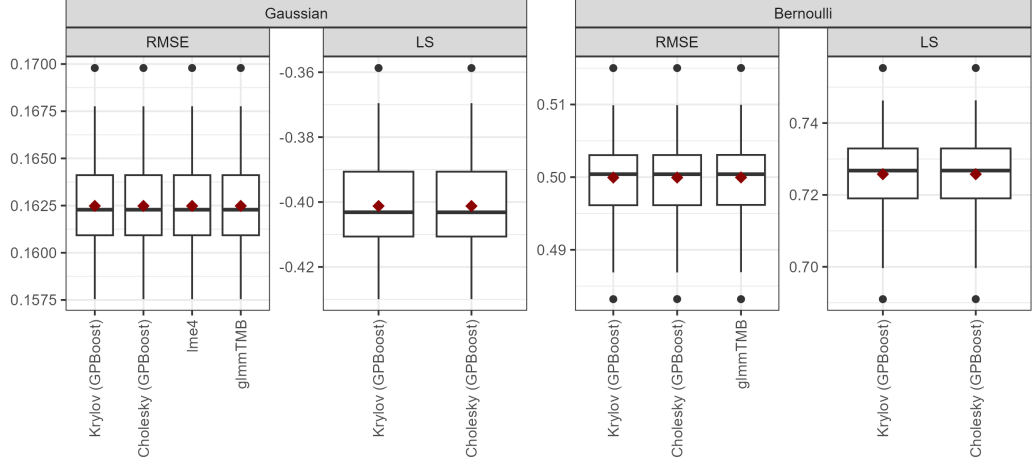


Figure 5: RMSE for predictive means and log score (LS) for probabilistic predictions for Gaussian and Bernoulli likelihoods.

## 6 Real-world applications

In this section, we conduct experiments on six real-world data sets with crossed random effects, analyzing the runtime and accuracy for parameter estimation. We compare the proposed Krylov subspace methods with Cholesky-based calculations implemented in the `GPBoost`, `lme4`, and `glmmTMB` packages, using the same model and computational settings as described in Section 5.1.

### 6.1 Data sets

We consider four regression ('cars', 'building\_permits', 'instEval', 'MovieLens\_32m') and two classification ('employee\_access', 'upselling') data sets. Table 1 gives an overview of the data sets reporting the sample size, the number of covariates included in a linear predictor, the categorical variables modeled using random effects including the number of group levels  $m_k$ , and the total number of non-zero entries in  $Z^T Z$ . In Figure 14 in Appendix A.10, we additionally visualize the non-zero entries of the matrix  $Z^T Z$  for the different data sets. For the 'MovieLens\_32m' data set [Harper and Konstan, 2015], we use linear and quadratic time trends as predictor variables. The data sets 'upselling' ('KD-DCup09\_upselling') and 'employee\_access' ('Amazon\_employee\_access') have previously been used by Pargent et al. [2022]. For more information on the 'instEval' and 'cars' data sets, we refer to Simchoni and Rosset [2023], and the data set 'building\_permits' ('chicago\_building\_permits') has been used by Reyes [2019]. In general, an extra category is added for missing values in categorical variables and numeric predictor variables are simply imputed using the mean. We use the ZIC preconditioner for the 'cars', 'building\_permits', and 'instEval' data sets and the SSOR preconditioner for the other data sets.

### 6.2 Results

Figure 6 shows the estimation runtimes for the different data sets. In Appendix A.10, we additionally report the wall-clock time, the log-marginal likelihood at the optimum, and the estimated parameters in tabular form. Parameter estimation crashes when using the `lme4` and `glmmTMB` packages on the 'upselling' data set. We have additionally tried modeling only the two variables Var216 and Var217 as random effects but still observed crashes on the 'upselling' data set. For the 'employee\_access' data set, we have also tried modeling the low-cardinality categorical variables such as 'role\_family' and 'role\_cat1' as dummy-coded fixed effects instead of random effects, but `glmmTMB` and `lme4` crash when

	data set	$n$	$p$	$K$	$y$	% 1	Cat. var.	$m_k$	$\text{nnz}(Z^T Z)$
Regression	cars	97,729	66	2	log(price)		model_id	15,226	185,807
							location_id	12,235	
	building_permits	527,168	6	3	log(cost)		contact_name	98,362	2,544,893
							latitude	206,197	
							longitude	206,170	
Classification	instEval	73,421	22	2	rating		student	2,972	150,942
							teacher	1,128	
	MovieLens_32m	32,000,204	2	2	rating		userId	200,948	64,285,788
							movieId	84,432	
	employee_access	32,769	0	9	approval	0.94	resource	7,518	469,262
							manager	4,243	
							role_cat1	128	
							role_cat2	177	
							role_dep.	449	
							role_title	343	
	upselling	50,000	34	4	up-selling	0.07	Var216	2,016	454,852
							Var217	13,991	
							Var198	4,291	
							Var199	5,074	

Table 1: Summary of real-world data sets.  $n$  is the number of samples,  $p$  is the number of predictor variables,  $K$  is the number of categorical variables modeled with random effects,  $y$  describes the response variable, ‘% 1’ is the frequency of the ‘1’s in the response variable for the classification data sets, ‘Cat. var.’ describes the categorical variables modeled with random effects,  $m_k$  is the number of group levels, and  $\text{nnz}(Z^T Z)$  is the number of non-zero entries in the matrix  $Z^T Z$ .

doing this. For the ‘MovieLens\_32m’ data set, **glmmTMB** and Cholesky-based computations in **GPBoost** crash due to memory errors. In Figure 7, we report the average differences in estimation runtime relative to the fastest method. For every method, the average is calculated over the data sets for which the method does not crash.

The results show that Krylov subspace methods clearly have the fastest runtime on all real-world data sets. Compared with Cholesky-based calculations using the **GPBoost** package, the average speedup of the Krylov subspace methods exceeds a factor of 25 on those data sets for which Cholesky-based calculations are feasible. On the relatively high-dimensional ‘building\_permits’ data set, parameter estimation with Krylov subspace methods is approximately 60 times faster compared to Cholesky-based calculations. On average, estimation with **lme4** and **glmmTMB** is approximately 220 and 85 times slower, respectively, than with the Krylov subspace-based methods. As observed in experiments with simulated data, **lme4** is slow on classification data and can crash, e.g., on the ‘upselling’ data set. Furthermore, estimation on the ‘MovieLens\_32m’ data set takes approximately 1,000 times longer with **lme4** than with Krylov subspace-based methods. Concerning the parameter estimates reported in Tables 8 and 7 in Appendix A.10, we find that all methods and packages yield essentially the same estimates except for **lme4** on the ‘building\_permits’ and ‘employee\_access’ data sets. In summary, our novel Krylov subspace-based methods are substantially faster than Cholesky-based calculations and numerically more stable.

## 7 Conclusion

We present Krylov subspace methods for mixed effects models with high-dimensional crossed random effects. We derive novel theoretical results on the convergence and accuracy of these methods, and we analyze them empirically. In experiments, we find that Krylov subspace-based methods are much faster and more stable than Cholesky-based calculations and other state-of-the-art software implementations

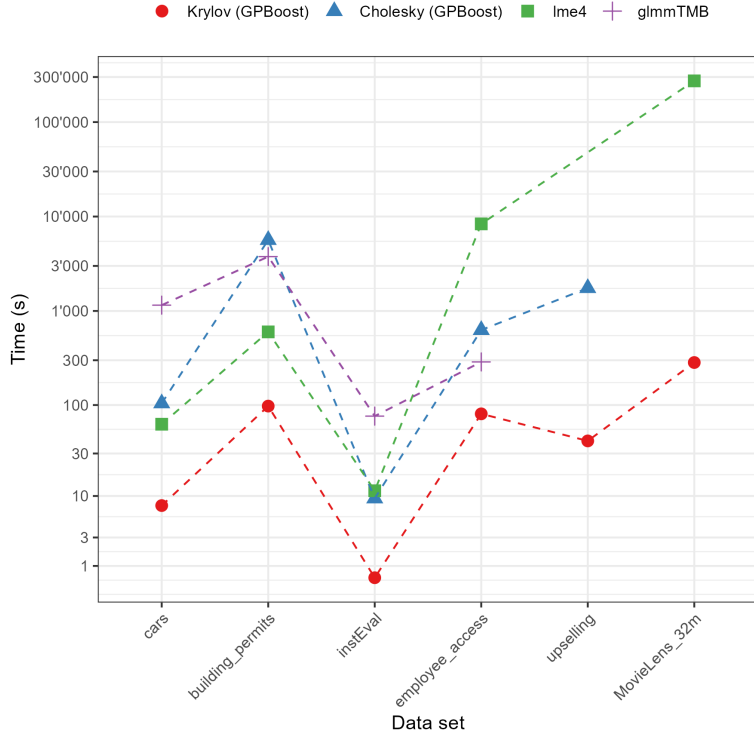


Figure 6: Runtimes for estimation on different real-world data sets for different models.

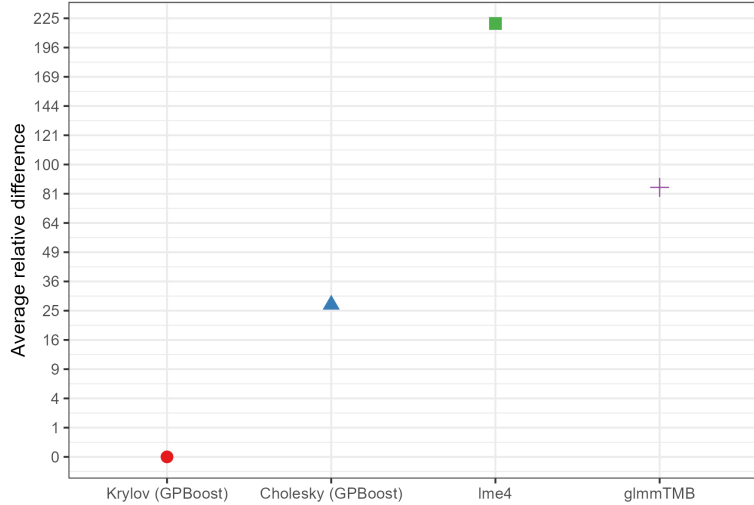


Figure 7: Average relative difference in runtime to the fastest model for the real-world data sets.

for GLMMs. For instance, we are able to estimate a model with two crossed random effects and three linear regression coefficients on the large-scale MovieLens\_32m data set in less than five minutes, whereas `lme4` requires more than three days and Cholesky-based computations in `glmmTMB` and `GPBoost` fail due to memory limitations.

We have used the Laplace approximation for non-Gaussian likelihoods following a common practice in widely used software implementations such as `lme4` and `glmmTMB`. A potential caveat of this is that, depending on the asymptotic setting for mixed effects models, the Laplace approximation can be biased [Shun and McCullagh, 1995]. Directions for future research include extending our methods to other marginal likelihood approximations, analyzing alternative approximations for log-determinants,

a systematic comparison under which situations the ZIC or the SSOR preconditioners are preferred, and the development of novel preconditioners.

## Acknowledgments

This research was partially supported by the Swiss Innovation Agency - Innosuisse (grant number '55463.1 IP-ICT').

## References

B. Avanzi, G. Taylor, M. Wang, and B. Wong. Machine learning with high-cardinality categorical features in actuarial applications. *ASTIN Bulletin: The Journal of the IAA*, 54(2):213–238, 2024.

D. Bates, M. Mächler, B. Bolker, and S. Walker. Fitting linear mixed-effects models using lme4. *Journal of statistical software*, 67:1–48, 2015.

C. Bekas, E. Kokiopoulou, and Y. Saad. An estimator for the diagonal of a matrix. *Applied numerical mathematics*, 57(11-12):1214–1229, 2007.

R. Bellio, S. Ghosh, A. B. Owen, and C. Varin. Consistent and scalable composite likelihood estimation of probit models with crossed random effects. *arXiv preprint arXiv:2308.15681*, 2023.

R. Border and S. Becker. Stochastic lanczos estimation of genomic variance components for linear mixed-effects models. *BMC bioinformatics*, 20:1–16, 2019.

G. Brito, I. Dumitriu, and K. D. Harris. Spectral gap in random bipartite biregular graphs and applications. *Combinatorics, Probability and Computing*, 31(2):229–267, 2022.

M. E. Brooks, K. Kristensen, K. J. v. Benthem, A. Magnusson, C. W. Berg, A. Nielsen, H. J. Skaug, M. Mächler, and B. M. Bolker. glmmTMB balances speed and flexibility among packages for zero-inflated generalized linear mixed modeling. *The R Journal*, 9:378–400, 2017. ISSN 2073-4859. doi: 10.32614/RJ-2017-066.

J. Cheng, C. Maltecca, P. M. VanRaden, J. R. O’Connell, L. Ma, and J. Jiang. Slemm: million-scale genomic predictions with window-based snp weighting. *Bioinformatics*, 39(3):btad127, 2023.

F. R. Chung. *Spectral graph theory*, volume 92. American Mathematical Soc., 1997.

K. Dong, D. Eriksson, H. Nickisch, D. Bindel, and A. G. Wilson. Scalable log determinants for gaussian process kernel learning. *Advances in Neural Information Processing Systems*, 30, 2017.

W. Fu and J. S. Simonoff. Unbiased regression trees for longitudinal and clustered data. *Computational Statistics & Data Analysis*, 88:53–74, 2015.

K. Gao and A. Owen. Efficient moment calculations for variance components in large unbalanced crossed random effects models. *Electronic Journal of Statistics*, 11:1235–1296, 2017.

K. Gao and A. B. Owen. Estimation and inference for very large linear mixed effects models. *Statistica Sinica*, 30(4):1741–1771, 2020.

J. Gardner, G. Pleiss, K. Q. Weinberger, D. Bindel, and A. G. Wilson. Gpytorch: Blackbox matrix-matrix gaussian process inference with gpu acceleration. *Advances in neural information processing systems*, 31, 2018.

D. J. Garrick, B. L. Golden, and D. P. Garrick. Alternative implementations of preconditioned conjugate gradient algorithms for solving mixed model equations. page 250–253, Armidale, 2019. Association for the Advancement of Animal Breeding and Genetics.

S. Ghosh, T. Hastie, and A. B. Owen. Backfitting for large scale crossed random effects regressions. *The Annals of Statistics*, 50(1):560–583, 2022a.

S. Ghosh, T. Hastie, and A. B. Owen. Scalable logistic regression with crossed random effects. *Electronic Journal of Statistics*, 16(2):4604–4635, 2022b.

G. H. Golub and C. F. Van Loan. *Matrix computations*. JHU press, 2013.

M. Goplerud, O. Papaspiliopoulos, and G. Zanella. Partially factorized variational inference for high-dimensional mixed models. *Biometrika*, page asae067, 2025.

T. Gyger, R. Furrer, and F. Sigrist. Iterative methods for full-scale gaussian process approximations for large spatial data. *arXiv preprint arXiv:2405.14492*, 2024.

A. Hajjem, F. Bellavance, and D. Larocque. Mixed effects regression trees for clustered data. *Statistics & probability letters*, 81(4):451–459, 2011.

A. Hajjem, F. Bellavance, and D. Larocque. Mixed-effects random forest for clustered data. *Journal of Statistical Computation and Simulation*, 84(6):1313–1328, 2014.

H. Harbrecht, M. Peters, and R. Schneider. On the low-rank approximation by the pivoted Cholesky decomposition. *Applied numerical mathematics*, 62(4):428–440, 2012.

F. M. Harper and J. A. Konstan. The movielens datasets: History and context. *Acm transactions on interactive intelligent systems (tiis)*, 5(4):1–19, 2015.

R. A. Horn and C. R. Johnson. *Matrix analysis*. Cambridge university press, 2012.

S. Kim, R. Pasupathy, and S. G. Henderson. A guide to sample average approximation. *Handbook of simulation optimization*, pages 207–243, 2015.

P. Kündig and F. Sigrist. Iterative methods for vecchia-Laplace approximations for latent Gaussian process models. *Journal of the American Statistical Association*, 120(550):1267–1280, 2025.

C. E. McCulloch and S. R. Searle. *Generalized, linear, and mixed models*. John Wiley & Sons, 2004.

A. Nishimura and M. A. Suchard. Prior-preconditioned conjugate gradient method for accelerated gibbs sampling in “large n, large p” bayesian sparse regression. *Journal of the American Statistical Association*, pages 1–14, 2022.

A. Pandolfi, O. Papaspiliopoulos, and G. Zanella. Conjugate gradient methods for high-dimensional GLMMs. *Journal of the American Statistical Association*, (in press):1–25, 2025.

O. Papaspiliopoulos, G. O. Roberts, and G. Zanella. Scalable inference for crossed random effects models. *Biometrika*, 107(1):25–40, 2020.

O. Papaspiliopoulos, T. Stumpf-Fétizon, and G. Zanella. Scalable bayesian computation for crossed and nested hierarchical models. *Electronic Journal of Statistics*, 17(2):3575–3612, 2023.

F. Pargent, F. Pfisterer, J. Thomas, and B. Bischl. Regularized target encoding outperforms traditional methods in supervised machine learning with high cardinality features. *Computational Statistics*, 37(5):2671–2692, 2022.

J. C. Pinheiro and D. M. Bates. Linear mixed-effects models: basic concepts and examples. *Mixed-effects models in S and S-Plus*, pages 3–56, 2000.

G. Pleiss, J. Gardner, K. Weinberger, and A. G. Wilson. Constant-time predictive distributions for gaussian processes. In *International Conference on Machine Learning*, pages 4114–4123. PMLR, 2018.

C. E. Rasmussen and C. K. Williams. *Gaussian processes for machine learning*. MIT Press Cambridge, MA, 2006.

P. C. Reyes. *Statistical learning with high-cardinality string categorical variables*. PhD thesis, Université Paris-Saclay, 2019.

Y. Saad. *Iterative methods for sparse linear systems*. SIAM, 2003.

J. Scott and M. Tůma. On positive semidefinite modification schemes for incomplete cholesky factorization. *SIAM Journal on Scientific computing*, 36(2):A609–A633, 2014.

R. J. Sela and J. S. Simonoff. Re-em trees: a data mining approach for longitudinal and clustered data. *Machine learning*, 86:169–207, 2012.

Z. Shun and P. McCullagh. Laplace approximation of high dimensional integrals. *Journal of the Royal Statistical Society Series B: Statistical Methodology*, 57(4):749–760, 1995.

F. Sigrist. Gaussian Process Boosting. *Journal of Machine Learning Research*, 23(232):1–46, 2022.

F. Sigrist. Latent Gaussian model boosting. *IEEE Transactions on Pattern Analysis and Machine Intelligence*, 45(2):1894–1905, 2023a.

F. Sigrist. A comparison of machine learning methods for data with high-cardinality categorical variables. *arXiv preprint arXiv:2307.02071*, 2023b.

G. Simchoni and S. Rosset. Using random effects to account for high-cardinality categorical features and repeated measures in deep neural networks. *Advances in Neural Information Processing Systems*, 34:25111–25122, 2021.

G. Simchoni and S. Rosset. Integrating random effects in deep neural networks. *Journal of Machine Learning Research*, 24(156):1–57, 2023.

I. Strandén and M. Lidauer. Solving large mixed linear models using preconditioned conjugate gradient iteration. *Journal of Dairy Science*, 82(12):2779–2787, 1999.

I. Strandén and M. Lidauer. Parallel computing applied to breeding value estimation in dairy cattle. *Journal of dairy science*, 84(1):276–285, 2001.

M. Taskinen, E. A. Mäntysaari, and I. Strandén. Single-step SNP-BLUP with on-the-fly imputed genotypes and residual polygenic effects. *Genetics Selection Evolution*, 49:1–15, 2017.

S. Tsuruta, I. Misztal, and I. Strandén. Use of the preconditioned conjugate gradient algorithm as a generic solver for mixed-model equations in animal breeding applications. *Journal of animal science*, 79(5):1166–1172, 2001.

S. Ubaru, J. Chen, and Y. Saad. Fast estimation of  $\text{tr}(f(a))$  via stochastic Lanczos quadrature. *SIAM Journal on Matrix Analysis and Applications*, 38(4):1075–1099, 2017.

A. Van der Sluis and H. A. van der Vorst. The rate of convergence of conjugate gradients. *Numerische Mathematik*, 48:543–560, 1986.

H. A. Van der Vorst. *Iterative Krylov methods for large linear systems*. Number 13. Cambridge University Press, 2003.

J. Vandeplassche, H. Eding, M. P. Calus, and C. Vuik. Deflated preconditioned conjugate gradient method for solving single-step BLUP models efficiently. *Genetics Selection Evolution*, 50:1–17, 2018.

J. Wenger, G. Pleiss, P. Hennig, J. Cunningham, and J. Gardner. Preconditioning for scalable Gaussian process hyperparameter optimization. In *International Conference on Machine Learning*, pages 23751–23780. PMLR, 2022.

K. Wu and H. Simon. Thick-restart Lanczos method for large symmetric eigenvalue problems. *SIAM Journal on Matrix Analysis and Applications*, 22(2):602–616, 2000.

L. Xu, N. Reid, and D. Kong. Gaussian variational approximation with composite likelihood for crossed random effect models. *arXiv preprint arXiv:2310.12485*, 2023.

## A Appendix

### A.1 Proofs of results in Section 4

**Notation.** We denote by  $\sigma_{\min}(B) = \sigma_{\min(n_1, n_2)}(B) \leq \dots \leq \sigma_1(B) = \sigma_{\max}(B)$  the singular values of a matrix  $B \in \mathbb{R}^{n_1 \times n_2}$ , and by  $\lambda_{\min}(A) = \lambda_m(A) \leq \dots \leq \lambda_1(A) = \lambda_{\max}(A)$  the eigenvalues of a symmetric matrix  $A \in \mathbb{R}^{m \times m}$ . Further, let

$$D = \Sigma^{-1} + \text{diag}(Z^T W Z) \in \mathbb{R}^{m \times m},$$

$$\Delta = \text{diag}(Z^T W Z) \in \mathbb{R}^{m \times m},$$

and

$$\Lambda = Z^T W Z - \text{diag}(Z^T W Z) \in \mathbb{R}^{m \times m}.$$

We will use the following two lemmas for proving Lemma 4.1.

**Lemma A.1.** For any  $B \in \mathbb{R}^{n_1 \times n_2}$  and  $A = \begin{pmatrix} 0 & B^T \\ B & 0 \end{pmatrix} \in \mathbb{R}^{(n_1+n_2) \times (n_1+n_2)}$ , the non-zero eigenvalues of  $A$  are equal to  $\pm$  the singular values of  $B$ , i.e.,

$$\{\lambda_i(A); i = 1, \dots, 2 \min(n_1, n_2)\} = \{\pm \sigma_i(B); i = 1, \dots, \min(n_1, n_2)\}.$$

In particular, the largest singular value of  $B$  and the largest eigenvalue of  $A$  are equal,  $\lambda_{\max}(A) = \sigma_{\max}(B)$ . The same holds true for the second largest singular value and eigenvalue.

*Proof of Lemma A.1.* The eigenvalues of  $A$  are defined as solutions to

$$\det(A - \lambda I) = 0.$$

Since  $A - \lambda I$  is a block matrix, we have

$$\det(A - \lambda I) = \det(\lambda^2 I - B^T B).$$

The eigenvalues of  $A$  are thus given by

$$\{\pm \sqrt{\lambda_i(B^T B)}; i = 1, \dots, \min(n_1, n_2)\} = \{\pm \sigma_i(B); i = 1, \dots, \min(n_1, n_2)\}.$$

□

**Lemma A.2.** For any matrix  $B \in \mathbb{R}^{n_1 \times n_2}$  and diagonal matrices  $C_1^{n_1 \times n_1}$  and  $C_2^{n_2 \times n_2}$ , it holds that

$$\sigma_{\max}(B) \min(|(C_1)_{ii}|) \min(|(C_2)_{jj}|) \leq \sigma_{\max}(C_1 B C_2) \leq \sigma_{\max}(B) \max(|(C_1)_{ii}|) \max(|(C_2)_{jj}|).$$

*Proof of Lemma A.2.*

$$\sigma_{\max}(C_1 B C_2) = \|C_1 B C_2\|_2 \leq \|C_1\|_2 \|B\|_2 \|C_2\|_2 = \sigma_{\max}(B) \max(|(C_1)_{ii}|) \max(|(C_2)_{jj}|).$$

Furthermore,

$$\sigma_{\max}(B) = \|B\|_2 = \|C_1^{-1} C_1 B C_2 C_2^{-1}\|_2 \leq \sigma_{\max}(C_1 B C_2) \frac{1}{\min(|(C_1)_{ii}|)} \frac{1}{\min(|(C_2)_{ii}|)}$$

which gives the first inequality.

□

*Proof of Lemma 4.1.* For the SSOR preconditioner  $P_{\text{SSOR}} = (L + D)D^{-1}(L + D)^T$ , we have

$$L = \begin{pmatrix} 0 & 0 \\ Z_2^T W Z_1 & 0 \end{pmatrix}, \quad D = \begin{pmatrix} D_1 & 0 \\ 0 & D_2 \end{pmatrix}, \quad \Sigma^{-1} + Z^T W Z = \begin{pmatrix} D_1 & Z_1^T W Z_2 \\ Z_2^T W Z_1 & D_2 \end{pmatrix}.$$

It can easily be seen that

$$(D + L)^{-1} = \begin{pmatrix} D_1^{-1} & 0 \\ -D_2^{-1} Z_2^T W Z_1 D_1^{-1} & D_2^{-1} \end{pmatrix},$$

and we thus obtain

$$\begin{aligned} P_{\text{SSOR}}^{-1/2}(\Sigma^{-1} + Z^T W Z) P_{\text{SSOR}}^{-T/2} &= D^{1/2}(D + L)^{-1}(\Sigma^{-1} + Z^T W Z)(D + L)^{-T} D^{1/2} \\ &= I_m - \begin{pmatrix} 0 & 0 \\ 0 & D_2^{-1/2} Z_2^T W Z_1 D_1^{-1} Z_1^T W Z_2 D_2^{-1/2} \end{pmatrix}. \end{aligned} \quad (40)$$

Because  $D_2^{-1/2} Z_2^T W Z_1 D_1^{-1} Z_1^T W Z_2 D_2^{-1/2}$  is a symmetric positive semi-definite matrix and using the fact that  $\lambda_i(I_m + A) = 1 + \lambda_i(A)$  for any normal matrix  $A$ , we obtain (21).

Using Lemma A.1, we have

$$\begin{aligned} \sigma_{\max}(D_2^{-1/2} Z_2^T W Z_1 D_1^{-1/2}) &= \lambda_{\max} \begin{pmatrix} 0 & D_1^{-1/2} Z_1^T W Z_2 D_2^{-1/2} \\ D_2^{-1/2} Z_2^T W Z_1 D_1^{-1/2} & 0 \end{pmatrix} \\ &= \lambda_{\max}(D^{-1/2} \Lambda D^{-1/2}) \\ &= \lambda_{\max}(D^{-1/2} \Delta^{1/2} \Delta^{-1/2} \Lambda \Delta^{-1/2} \Delta^{1/2} D^{-1/2}). \end{aligned}$$

Note that  $\Delta^{-1/2} \Lambda \Delta^{-1/2}$  is a normalized adjacency matrix of a bipartite weighted graph. Its largest eigenvalues is thus 1 [Chung, 1997]. By Lemma A.2, or Ostrowski's theorem [Horn and Johnson, 2012], it follows that

$$\min((D^{-1} \Delta)_{ii}) \leq \sigma_{\max}(D_2^{-1/2} Z_2^T W Z_1 D_1^{-1/2}) \leq \max((D^{-1} \Delta)_{ii}).$$

Since  $D^{-1} \Delta = \text{diag} \left( \frac{1}{\Sigma_{ii}^{-1} \Delta_{ii}^{-1} + 1} \right)$  and

$$\lambda_i(D_2^{-1/2} Z_2^T W Z_1 D_1^{-1} Z_1^T W Z_2 D_2^{-1/2}) = \sigma_i(D_2^{-1/2} Z_2^T W Z_1 D_1^{-1/2})^2, \quad 1 \leq i \leq \min(m_1, m_2), \quad (41)$$

we have

$$\frac{1}{(\max(\Sigma_{ii}^{-1} \Delta_{ii}^{-1}) + 1)^2} \leq \lambda_{\max}(D_2^{-1/2} Z_2^T W Z_1 D_1^{-1} Z_1^T W Z_2 D_2^{-1/2}) \leq \frac{1}{(\min(\Sigma_{ii}^{-1} \Delta_{ii}^{-1}) + 1)^2},$$

from which follows (22).

Furthermore, since

$$\sigma_{\max}(Z_2^T W Z_1) = \lambda_{\max} \begin{pmatrix} 0 & Z_1^T W Z_2 \\ Z_2^T W Z_1 & 0 \end{pmatrix} = \lambda_{\max}(\Lambda) = \lambda_{\max}(\Delta^{1/2} \Delta^{-1/2} \Lambda \Delta^{-1/2} \Delta^{1/2}).$$

and applying Lemma A.2, we obtain

$$\min(\Delta_{ii}) \leq \sigma_{\max}(Z_2^T W Z_1) \leq \max(\Delta_{ii}).$$

By again using Lemma A.2, we obtain

$$\min((D_1^{-1/2})_{ii}) \min((D_2^{-1/2})_{ii}) \min(\Delta_{ii}) \leq \sigma_{\max}(D_2^{-1/2} Z_2^T W Z_1 D_1^{-1/2}) \leq \max((D_1^{-1/2})_{ii}) \max((D_2^{-1/2})_{ii}) \max(\Delta_{ii})$$

and

$$\min((D_1)_{ii}^{-1}) \min((D_2)_{ii}^{-1}) \min(\Delta_{ii}^2) \leq \lambda_{\max}(D_2^{-1/2} Z_2^T W Z_1 D_1^{-1} Z_1^T W Z_2 D_2^{-1/2}) \leq \max((D_1)_{ii}^{-1}) \max((D_2)_{ii}^{-1}) \max(\Delta_{ii}^2)$$

which gives the second set of inequalities for  $\lambda_{\min}^{\text{SSOR}}$  in (23).  $\square$

*Proof of Lemma 4.2.* Consider the vectors

$$v_k = D^{1/2} \left( \frac{1}{k} 1_{m_1}^T, \dots, \frac{1}{k} 1_{m_k}^T, -1_{m_{k+1}}^T, 0, \dots, 0 \right)^T \in \mathbb{R}^m, \quad k = 1, \dots, K-1,$$

where  $1_{m_k}$  denotes a vectors of 1's of length  $m_k$ . We have  $D^{-1/2} Z^T W Z D^{-1/2} v_k = 0$ , and the vectors  $v_k$  are linearly independent. Since  $D^{-1/2} Z^T W Z D^{-1/2}$  is positive semi-definite, this shows that the

$K - 1$  smallest eigenvalues of  $D^{-1/2}Z^T W Z D^{-1/2}$  are zero. Applying Weyl's inequality [Horn and Johnson, 2012] to  $P_{\text{Diag}}^{-1/2}(\Sigma^{-1} + Z^T W Z)P_{\text{Diag}}^{-T/2} = D^{-1/2}\Sigma^{-1}D^{-1/2} + D^{-1/2}Z^T W Z D^{-1/2}$  gives

$$\lambda_{\min}(D^{-1/2}\Sigma^{-1}D^{-1/2}) \leq \lambda_{m+1-k}(P_{\text{Diag}}^{-1/2}(\Sigma^{-1} + Z^T W Z)P_{\text{Diag}}^{-T/2}) \leq \lambda_{\max}(D^{-1/2}\Sigma^{-1}D^{-1/2})$$

for  $k = 1, \dots, K - 1$ , which proves (25).

Similarly as in the proof of Lemma 4.1, we can show, for general  $K$ , that

$$(K - 1) \min((D^{-1}\Delta)_{ii}) \leq \lambda_{\max}(D^{-1/2}\Lambda D^{-1/2}) \leq (K - 1) \max((D^{-1}\Delta)_{ii}). \quad (42)$$

For doing this, we first note that  $\Lambda$  is an adjacency matrix of a connected,  $K$ -partite weighted graph. Moreover,

$$\begin{aligned} \sum_{j=1}^m \Lambda_{ij} &= \sum_{k=1, k \neq \tilde{k}(i)}^K \sum_{j=1}^{m_k} (Z_{\tilde{k}(i)}^T W Z_k)_{ij} \\ &= \sum_{k=1, k \neq \tilde{k}(i)}^K \sum_{j=1}^{m_k} \sum_{l=1}^n W_{ll} (Z_{\tilde{k}(i)})_{li} (Z_k)_{lj} \\ &= \sum_{k=1, k \neq \tilde{k}(i)}^K \sum_{l=1}^n W_{ll} (Z_{\tilde{k}(i)})_{li} \\ &= \sum_{k=1, k \neq \tilde{k}(i)}^K \Delta_{ii} = (K - 1)\Delta_{ii} \end{aligned}$$

where  $\tilde{k}(i) = k$  if  $i \in \{\sum_{k'=0}^{k-1} m_{k'} + 1, \dots, \sum_{k'=0}^k m_{k'}\}$  with the convention  $m_0 = 0$ . This shows that  $\frac{1}{K-1}\Delta^{-1/2}\Lambda\Delta^{-1/2}$  is a normalized adjacency matrix of a connected,  $K$ -partite weighted graph whose largest eigenvalue is 1. Using

$$\lambda_{\max}(D^{-1/2}\Lambda D^{-1/2}) = (K - 1)\lambda_{\max}(D^{-1/2}\Delta^{1/2} \frac{1}{K-1}\Delta^{-1/2}\Lambda\Delta^{-1/2}\Delta^{1/2}D^{-1/2})$$

gives (42), which together with

$$P_{\text{Diag}}^{-1/2}(\Sigma^{-1} + Z^T W Z)P_{\text{Diag}}^{-T/2} = I_m + D^{-1/2}\Lambda D^{-1/2} \quad (43)$$

proves the statement in (24).

Next, we have

$$\Sigma^{-1} + Z^T W Z = \Sigma^{-1} + \Delta^{1/2}(I_m + \Delta^{-1/2}\Lambda\Delta^{-1/2})\Delta^{1/2}.$$

Applying Weyl's inequality [Horn and Johnson, 2012], Ostrowski's theorem [Horn and Johnson, 2012], and the fact that the largest eigenvalue of  $\Delta^{-1/2}\Lambda\Delta^{-1/2}$  is  $K - 1$ , see above, we obtain (26). (27) is shown analogously as (25) above.  $\square$

For proofing parts of Theorem 4.2, we first derive the following slightly more general result.

**Theorem A.1.** *If the likelihood is Gaussian, it holds that*

$$1 + \frac{K - 1}{\frac{\max(\Sigma^{-1})\sigma^2}{d_{\min}} + 1} \leq \lambda_{\max}^{\text{Diag}} \leq 1 + \frac{K - 1}{\frac{\min(\Sigma^{-1})\sigma^2}{d_{\max}} + 1}, \quad (44)$$

$$\frac{1}{\frac{\max(\Sigma)}{\sigma^2} d_{\max} + 1} \leq \lambda_{m+1-k}^{\text{Diag}} \leq \frac{1}{\frac{\min(\Sigma)}{\sigma^2} d_{\min} + 1}, \quad k = 1, \dots, K - 1, \quad (45)$$

where  $d_{\max} = \max(Z^T Z)$  and  $d_{\min} = \min(Z^T Z)$ .

If, in addition,  $K = 2$  and the design of the random effects is balanced in the sense that every random effect occurs  $d_k$  times for component  $k = 1, 2$ , i.e.,  $d_k = \frac{n}{m_k} = \sum_{i=1}^n (Z_k)_{ij}$  for all  $1 \leq j \leq m_k$ , it holds that

$$\lambda_{\max}^{Diag} = 1 + \frac{1}{\sqrt{\left(\frac{\sigma^2}{\sigma_1^2 d_1} + 1\right) \left(\frac{\sigma^2}{\sigma_2^2 d_2} + 1\right)}} \quad (46)$$

$$\lambda_{\min}^{Diag} = 1 - \frac{1}{\sqrt{\left(\frac{\sigma^2}{\sigma_1^2 d_1} + 1\right) \left(\frac{\sigma^2}{\sigma_2^2 d_2} + 1\right)}} \quad (47)$$

*Proof of Theorem A.1.* First, (44) and (45) follow directly from (24) and (25).

For deriving (46), note that

$$\begin{aligned} D^{-1/2} \Delta^{1/2} &= \text{diag} \left( \frac{1}{\Sigma_{ii}^{-1} \Delta_{ii}^{-1} + 1} \right)^{1/2} \\ &= \text{diag} \left( \frac{1}{\sqrt{\frac{\sigma^2}{\sigma_1^2 d_1} + 1}}, \dots, \frac{1}{\sqrt{\frac{\sigma^2}{\sigma_1^2 d_1} + 1}}, \frac{1}{\sqrt{\frac{\sigma^2}{\sigma_2^2 d_2} + 1}}, \dots, \frac{1}{\sqrt{\frac{\sigma^2}{\sigma_2^2 d_2} + 1}} \right), \end{aligned}$$

which implies

$$D^{-1/2} \Delta^{1/2} \Delta^{-1/2} \Lambda \Delta^{-1/2} \Delta^{1/2} D^{-1/2} = \frac{1}{\sqrt{\frac{\sigma^2}{\sigma_1^2 d_1} + 1}} \frac{1}{\sqrt{\frac{\sigma^2}{\sigma_2^2 d_2} + 1}} \Delta^{-1/2} \Lambda \Delta^{-1/2}. \quad (48)$$

Using  $\lambda_{\max}(\Delta^{-1/2} \Lambda \Delta^{-1/2}) = K - 1$ , see the proof of Lemma 4.2, then gives

$$\begin{aligned} \lambda_{\max}(D^{-1/2} \Lambda D^{-1/2}) &= \lambda_{\max}(D^{-1/2} \Delta^{1/2} \Delta^{-1/2} \Lambda \Delta^{-1/2} \Delta^{1/2} D^{-1/2}) \\ &= \frac{K - 1}{\sqrt{\frac{\sigma^2}{\sigma_1^2 d_1} + 1} \sqrt{\frac{\sigma^2}{\sigma_2^2 d_2} + 1}}. \end{aligned}$$

This and (43) proof (46).

By analogous arguments, again using (48) and  $\lambda_{\min}(\Delta^{-1/2} \Lambda \Delta^{-1/2}) = -1$  due to Lemma A.1, we have

$$\lambda_{\min}(D^{-1/2} \Lambda D^{-1/2}) = -\frac{1}{\sqrt{\frac{\sigma^2}{\sigma_1^2 d_1} + 1}} \frac{1}{\sqrt{\frac{\sigma^2}{\sigma_2^2 d_2} + 1}},$$

which gives (47).  $\square$

*Proof of Theorem 4.2.* First, (22) and

$$\min(\Sigma_{ii}^{-1} (Z^T W Z)_{ii}^{-1}) \geq \min(\Sigma^{-1})_{ii} \min((Z^T W Z)_{ii}^{-1}) = \frac{\sigma^2}{\sigma_{\max}^2 d_{\max}}$$

imply

$$1 - \left( \frac{\sigma_{\max}^2 d_{\max}}{\sigma^2 + \sigma_{\max}^2 d_{\max}} \right)^2 \leq \lambda_{\min}^{\text{SSOR}} \leq 1 - \left( \frac{\sigma_{\min}^2 d_{\min}}{\sigma^2 + \sigma_{\min}^2 d_{\min}} \right)^2$$

which gives (28). In addition,

$$\frac{1}{1 - \left( \frac{\sigma_{\max}^2 d_{\max}}{\sigma^2 + \sigma_{\max}^2 d_{\max}} \right)^2} = \frac{1}{2} \frac{\sigma_{\max}^2 d_{\max}}{\sigma^2} + \frac{3}{4} + \frac{1}{8\sigma_{\max}^2 d_{\max}/\sigma^2 + 4}$$

yields the asymptotic result in (28).

Furthermore, plugging in  $D_k = \text{diag}(1/\sigma_k^2 + d_k/\sigma^2)$ ,  $k = 1, 2$ , in (23) gives

$$\frac{\lambda_{\max}^{\text{SSOR}}}{\lambda_{\min}^{\text{SSOR}}} = \frac{1}{1 - \left( \frac{1}{\frac{\sigma_1^2}{\sigma^2} d + 1} \right) \left( \frac{1}{\frac{\sigma_2^2}{\sigma^2} d + 1} \right)} = \frac{1}{\frac{(\sigma^2)^2 + \sigma^2(\sigma_1^2 + \sigma_2^2)d}{(\sigma^2)^2 + \sigma^2(\sigma_1^2 + \sigma_2^2)d + \sigma_1^2 \sigma_2^2 d^2}} = \frac{(\sigma^2)^2/d + \sigma^2(\sigma_1^2 + \sigma_2^2) + \sigma_1^2 \sigma_2^2 d}{(\sigma^2)^2/d + \sigma^2(\sigma_1^2 + \sigma_2^2)},$$

which yields

$$\lim_{d \rightarrow \infty} \left( \frac{\lambda_{\max}^{\text{SSOR}}}{\lambda_{\min}^{\text{SSOR}}} - \left( \frac{\sigma_1^2 \sigma_2^2}{\sigma^2(\sigma_1^2 + \sigma_2^2)} d + 1 \right) \right) = 0$$

and thus proves the statements in (31).

Next, Theorem A.1 implies

$$\left( 1 + \frac{1}{\frac{\sigma^2}{\sigma_{\min}^2 d_{\min}} + 1} \right) \left( \frac{\sigma_{\min}^2 d_{\min}}{\sigma^2} + 1 \right) \leq \frac{\lambda_{\max}^{\text{Diag}}}{\lambda_{\min}^{\text{Diag}}} \leq \left( 1 + \frac{1}{\frac{\sigma^2}{\sigma_{\max}^2 d_{\max}} + 1} \right) \left( \frac{\sigma_{\max}^2 d_{\max}}{\sigma^2} + 1 \right),$$

which gives (29). Similarly, by Theorem A.1, we have

$$\frac{\lambda_{\max}^{\text{Diag}}}{\lambda_{\min}^{\text{Diag}}} = \frac{\left( 1 + \frac{1}{\sqrt{\left( \frac{\sigma^2}{\sigma_1^2 d} + 1 \right) \left( \frac{\sigma^2}{\sigma_2^2 d} + 1 \right)}} \right)}{\left( 1 - \frac{1}{\sqrt{\left( \frac{\sigma^2}{\sigma_1^2 d} + 1 \right) \left( \frac{\sigma^2}{\sigma_2^2 d} + 1 \right)}} \right)} = \frac{\sqrt{\left( \frac{\sigma^2}{\sigma_1^2 d} + 1 \right) \left( \frac{\sigma^2}{\sigma_2^2 d} + 1 \right)} + 1}{\sqrt{\left( \frac{\sigma^2}{\sigma_1^2 d} + 1 \right) \left( \frac{\sigma^2}{\sigma_2^2 d} + 1 \right)} - 1},$$

which is the first equality in (32). Using

$$\sqrt{\left( \frac{\sigma^2}{\sigma_1^2 d} + 1 \right) \left( \frac{\sigma^2}{\sigma_2^2 d} + 1 \right)} = 1 + \frac{1}{2} \left( \frac{\sigma^2}{\sigma_1^2 d} + \frac{\sigma^2}{\sigma_2^2 d} \right) + \mathcal{O}(d^{-2}),$$

one can show that  $\frac{\lambda_{\max}^{\text{Diag}}}{\lambda_{\min}^{\text{Diag}}}$  has the linear asymptote  $\frac{4\sigma_1^2 \sigma_2^2}{\sigma^2(\sigma_1^2 + \sigma_2^2)}$ , i.e.,

$$\lim_{d \rightarrow \infty} \left( \frac{\lambda_{\max}^{\text{Diag}}}{\lambda_{\min}^{\text{Diag}}} - \left( \frac{4\sigma_1^2 \sigma_2^2}{\sigma^2(\sigma_1^2 + \sigma_2^2)} d + 1 \right) \right) = 0.$$

Finally, (30) follows from Lemma 4.2.  $\square$

*Proof of Theorem 4.3.* We first note that

$$\begin{aligned} \min(\Sigma_{ii}^{-1} (Z^T W Z)^{-1}_{ii}) &\geq \frac{1}{\max(\Sigma)_{ii} \max((Z^T W Z)_{ii})} \\ &\geq \frac{1}{\max(\Sigma)_{ii} \max((Z^T Z)_{ii}) \max(W)} \\ &\geq \frac{1}{\sigma_{\max}^2 d_{\max} C}, \end{aligned} \tag{49}$$

since

$$\max(W) \leq C, \tag{50}$$

where  $C$  equals 0.25 and 1 for a logit and a probit link, respectively. This and (22) imply

$$1 - \left( \frac{\sigma_{\max}^2 d_{\max} C}{1 + \sigma_{\max}^2 d_{\max} C} \right)^2 \leq \lambda_{\min}^{\text{SSOR}},$$

which gives the inequality in (33). Similarly as in the proof of Theorem 4.2, we have

$$\frac{1}{1 - \left( \frac{\sigma_{\max}^2 d_{\max} C}{1 + \sigma_{\max}^2 d_{\max} C} \right)^2} = \frac{\sigma_{\max}^2 C}{2} d_{\max} + \frac{3}{4} + \frac{1}{8\sigma_{\max}^2 d_{\max} C + 4},$$

which yields the asymptotic result in (33).

For the diagonal preconditioner, (24) and the inequality in (49) imply

$$\lambda_{\max}^{\text{Diag}} \leq 1 + \frac{1}{\frac{1}{\sigma_{\max}^2 d_{\max} C} + 1} = \frac{2\sigma_{\max}^2 d_{\max} C + 1}{\sigma_{\max}^2 d_{\max} C + 1},$$

and (25) and (50) imply

$$\frac{1}{1 + \sigma_{\max}^2 d_{\max} C} \leq \lambda_{\min}^{\text{Diag}}.$$

This gives (34). For the unpreconditioned matrix, Lemma 4.2 and (50) imply (35).  $\square$

*Proof of Theorem 4.4.* Similarly as in the proof of Lemma 4.1, we can apply Lemma A.1 and obtain

$$\begin{aligned} \sigma_2 \left( \frac{1}{\sigma^2} D_2^{-1/2} Z_2^T Z_1 D_1^{-1/2} \right) &= \lambda_2 \left( \frac{1}{\sigma^2} D^{-1/2} \begin{pmatrix} 0 & Z_1^T Z_2 \\ Z_2^T Z_1 & 0 \end{pmatrix} D^{-1/2} \right) \\ &= \lambda_2 \left( \begin{pmatrix} 0 & Z_1^T Z_2 \\ Z_2^T Z_1 & 0 \end{pmatrix} \frac{1}{\sqrt{\sigma^2/\sigma_1^2 + d_1}} \frac{1}{\sqrt{\sigma^2/\sigma_2^2 + d_2}} \right), \end{aligned} \quad (51)$$

where we have used

$$\sigma^{-1} D^{-1/2} = \text{diag} \left( \frac{1}{\sqrt{\sigma^2/\sigma_1^2 + d_1}}, \dots, \frac{1}{\sqrt{\sigma^2/\sigma_1^2 + d_1}}, \frac{1}{\sqrt{\sigma^2/\sigma_2^2 + d_2}}, \dots, \frac{1}{\sqrt{\sigma^2/\sigma_2^2 + d_2}} \right).$$

Applying Theorem 3.2 of Brito et al. [2022] to  $\lambda_2 \left( \begin{pmatrix} 0 & Z_1^T Z_2 \\ Z_2^T Z_1 & 0 \end{pmatrix} \right)$  then shows that

$$\begin{aligned} \sigma_2 \left( \frac{1}{\sigma^2} D_2^{-1/2} Z_2^T Z_1 D_1^{-1/2} \right) &\leq \frac{\sqrt{d_1 - 1} + \sqrt{d_2 - 1}}{\sqrt{\sigma^2/\sigma_1^2 + d_1} \sqrt{\sigma^2/\sigma_2^2 + d_2}} + \epsilon'_m \\ &\leq \frac{1}{\sqrt{d_1}} + \frac{1}{\sqrt{d_2}} + \epsilon'_m \end{aligned}$$

asymptotically almost surely with  $\epsilon'_m \rightarrow 0$  as  $m \rightarrow \infty$ . Using (40) and (41) then give

$$\begin{aligned} \lambda_{m-1}^{\text{SSOR}} &\geq 1 - \frac{(\sqrt{d_1 - 1} + \sqrt{d_2 - 1})^2}{(\sigma^2/\sigma_1^2 + d_1)(\sigma^2/\sigma_2^2 + d_2)} - \epsilon_m \\ &\geq 1 - \left( \frac{1}{d_1} + \frac{1}{d_2} + \frac{2}{\sqrt{d_1 d_2}} \right) - \epsilon_m. \end{aligned} \quad (52)$$

Finally, (36) follows directly from (52).  $\square$

**Theorem A.2.** If  $K = 2$ , the likelihood is Gaussian, and  $\begin{pmatrix} 0 & Z_1^T Z_2 \\ Z_2^T Z_1 & 0 \end{pmatrix} \in \{0, 1\}^{m \times m}$  is an adjacency matrix of a bipartite, biregular random graph with uniform distribution over all bipartite, biregular random graphs, the following holds:

$$\kappa_{m-1,2}^{\text{Diag}} = \frac{\lambda_2^{\text{Diag}}}{\lambda_{m-1}^{\text{Diag}}} \leq \frac{1 + \frac{1}{\sqrt{d_1}} + \frac{1}{\sqrt{d_2}} + \epsilon_m}{1 - \left( \frac{1}{\sqrt{d_1}} + \frac{1}{\sqrt{d_2}} \right) - \epsilon_m} \quad (53)$$

asymptotically almost surely with  $\epsilon_m \rightarrow 0$  as  $m \rightarrow \infty$ , where  $d_k = \frac{n}{m_k}$  for  $k = 1, 2$ .

*Proof of Theorem A.2.* We have  $\lambda_2^{\text{Diag}} = 1 + \lambda_2(D^{-1/2} \Lambda D^{-1/2})$  because of (43). Next, (51) gives

$$\lambda_2(D^{-1/2} \Lambda D^{-1/2}) = \lambda_2 \left( \begin{pmatrix} 0 & Z_1^T Z_2 \\ Z_2^T Z_1 & 0 \end{pmatrix} \frac{1}{\sqrt{\sigma^2/\sigma_1^2 + d_1}} \frac{1}{\sqrt{\sigma^2/\sigma_2^2 + d_2}} \right).$$

Analogously as in the proof of Theorem 4.4, applying Theorem 3.2 of Brito et al. [2022] to  $\lambda_2 \left( \begin{pmatrix} 0 & Z_1^T Z_2 \\ Z_2^T Z_1 & 0 \end{pmatrix} \right)$  then shows that

$$\begin{aligned} \lambda_2^{\text{Diag}} &\leq 1 + \frac{\sqrt{d_1 - 1} + \sqrt{d_2 - 1}}{\sqrt{\sigma^2/\sigma_1^2 + d_1} \sqrt{\sigma^2/\sigma_2^2 + d_2}} + \epsilon_m \\ &\leq 1 + \frac{1}{\sqrt{d_1}} + \frac{1}{\sqrt{d_2}} + \epsilon_m \end{aligned}$$

asymptotically almost surely with  $\epsilon_m \rightarrow 0$  as  $m \rightarrow \infty$ . Lemma A.1 and analogous arguments give

$$\lambda_{m-1}^{\text{Diag}} \geq 1 - \left( \frac{1}{\sqrt{d_1}} + \frac{1}{\sqrt{d_2}} \right) - \epsilon_m.$$

The above two inequalities then result in (53).  $\square$

*Proof of Corollary 4.1.* Theorem 4.4 implies that

$$\kappa_{m-1,1}^{\text{SSOR}} \leq \frac{1}{1 - \frac{4}{d} - \epsilon_m}.$$

Applying the expansion  $(1-x)^{-1} = 1 + x + x^2 + O(x^3)$  with  $x = \frac{4}{d} + \epsilon_m$  gives (38). Similarly, Theorem A.2, applying the expansion  $(1-x)^{-1} = 1 + x + x^2 + O(x^3)$  in the denominator of  $\frac{1 + \frac{2}{\sqrt{d}} + \epsilon'_m}{1 - \frac{2}{\sqrt{d}} - \epsilon'_m}$ , and multiplying by the numerator  $1 + \frac{2}{\sqrt{d}} + \epsilon'_m$  give (39).  $\square$

## A.2 Proofs of Proposition 3.1, Proposition 3.2, and Proposition 3.3

*Proof of Proposition 3.1.* By standard results,  $\frac{1}{s} \sum_{i=1}^s z_i^{(1)} \odot z_i^{(2)} = \frac{1}{s} \sum_{i=1}^s z_i^{(1)} \odot Z_{po}(\Sigma^{-1} + Z^T W Z)^{-1} Z_{po}^T z_i^{(1)}$  in Algorithm 1 is an unbiased and consistent estimator for  $\text{diag}(Z_{po}(\Sigma^{-1} + Z^T W Z)^{-1} Z_{po}^T)$  and  $\frac{1}{s} \sum_{i=1}^s z_i^{(1)} \odot z_i^{(3)} = \frac{1}{s} \sum_{i=1}^s z_i^{(1)} \odot Z_{po} P^{-1} Z_{po}^T z_i^{(1)}$  is an unbiased and consistent estimator for  $\text{diag}(Z_{po} P^{-1} Z_{po}^T)$ . Thus, the claim in Proposition 3.1 follows.  $\square$

*Proof of Proposition 3.2.* First, observe that  $z_i^{(3)} = \Sigma^{-\frac{1}{2}} z_i^{(1)} + Z^T W^{\frac{1}{2}} z_i^{(2)} \sim \mathcal{N}(0, (\Sigma^{-1} + Z^T W Z))$ . It follows that  $z_i^{(4)} = Z_{po}(\Sigma^{-1} + Z^T W Z)^{-1} z_i^{(3)} \sim \mathcal{N}(0, Z_{po}(\Sigma^{-1} + Z^T W Z)^{-1} Z_{po}^T)$ . By standard results,  $\frac{1}{s} \sum_{i=1}^s z_i^{(4)} \left( z_i^{(4)} \right)^T$  in Algorithm 2 is an unbiased and consistent estimator for  $Z_{po}(\Sigma^{-1} + Z^T W Z)^{-1} Z_{po}^T$ , and the claim in Proposition 3.2 thus follows.  $\square$

*Proof of Proposition 3.3.* First, observe that  $z_i^{(3)} = Z \Sigma^{\frac{1}{2}} z_i^{(1)} + W^{-\frac{1}{2}} z_i^{(2)} \sim \mathcal{N}(0, \Psi)$ . It follows that  $z_i^{(4)} = Z_{po} \Sigma Z^T \Psi^{-1} z_i^{(3)} \sim \mathcal{N}(0, Z_{po} \Sigma Z^T \Psi^{-1} Z \Sigma Z_{po}^T)$ . By standard results,  $\frac{1}{s} \sum_{i=1}^s z_i^{(4)} \left( z_i^{(4)} \right)^T$  in Algorithm 3 is an unbiased and consistent estimator for  $Z_{po} \Sigma Z^T \Psi^{-1} Z \Sigma Z_{po}^T$ , and the claim in Proposition 3.3 thus follows.  $\square$

## A.3 Derivatives of log-determinants using stochastic trace estimation and variance reduction for SSOR preconditioner

In the following,  $c = \widehat{\text{Cov}}(h(z_i), r(z_i)) / \widehat{\text{Var}}(r(z_i))$  is the optimal weight for the variance reduction.

### A.3.1 Derivative for variance parameters

Note that  $\frac{\partial D}{\partial \theta_k} = \frac{\partial \Sigma^{-1}}{\partial \theta_k} = -\Sigma^{-1} \Sigma^{-1}$ .

$$\frac{\partial \log \det(\Sigma^{-1} + Z^T W Z)}{\partial \theta_k} \approx c \underbrace{\frac{\partial \log \det(P_{\text{SSOR}})}{\partial \theta_k}}_{\text{deterministic}} + \frac{\partial \log \det(\Sigma^{-1} + Z^T W Z)}{\partial \theta_k} - c \underbrace{\frac{\partial \log \det(P_{\text{SSOR}})}{\partial \theta_k}}_{\text{stochastic}}$$

$$\begin{aligned} \underbrace{\frac{\partial \log \det(P_{\text{SSOR}})}{\partial \theta_k}}_{\text{deterministic}} &= \frac{\partial (\log \det(L + D) + \log \det(D^{-1}) + \log \det(L + D))}{\partial \theta_k} \\ &= \frac{\partial \log \det(D)}{\partial \theta_k} \\ &= \text{tr} \left( D^{-1} \frac{\partial D}{\partial \theta_k} \right) \end{aligned}$$

$$\begin{aligned}
\frac{\partial \log \det(\Sigma^{-1} + Z^T W Z)}{\partial \theta_k} &= \text{tr} \left( (\Sigma^{-1} + Z^T W Z)^{-1} \frac{\partial(\Sigma^{-1} + Z^T W Z)}{\partial \theta_k} \right) \\
&= \text{tr} \left( (\Sigma^{-1} + Z^T W Z)^{-1} \frac{\partial \Sigma^{-1}}{\partial \theta_k} \right) \\
&= \text{tr} \left( -(\Sigma^{-1} + Z^T W Z)^{-1} \Sigma^{-1} \Sigma^{-1} \right) \\
&\approx \frac{1}{t} \sum_{i=1}^t \underbrace{-((\Sigma^{-1} + Z^T W Z)^{-1} z_i)^T \Sigma^{-1} \Sigma^{-1} P_{\text{SSOR}}^{-1} z_i}_{=: h(z_i)}
\end{aligned}$$

$$\begin{aligned}
\underbrace{\frac{\partial \log \det(P_{\text{SSOR}})}{\partial \theta_k}}_{\text{stochastic}} &= \text{tr} \left( P_{\text{SSOR}}^{-1} \frac{\partial P_{\text{SSOR}}}{\partial \theta_k} \right) \\
&= \text{tr} \left( P_{\text{SSOR}}^{-1} \frac{\partial(L + D) D^{-1} (L + D)^T}{\partial \theta_k} \right) \\
&= \text{tr} \left( P_{\text{SSOR}}^{-1} \left( 2 \frac{\partial D}{\partial \theta_k} D^{-1} (L + D)^T - (L + D) D^{-1} \frac{\partial D}{\partial \theta_k} D^{-1} (L + D)^T \right) \right) \\
&\approx \frac{1}{t} \sum_{i=1}^t \underbrace{(P_{\text{SSOR}}^{-1} z_i)^T \left( 2 \frac{\partial D}{\partial \theta_k} D^{-1} (L + D)^T - (L + D) D^{-1} \frac{\partial D}{\partial \theta_k} D^{-1} (L + D)^T \right) P_{\text{SSOR}}^{-1} z_i}_{=: r(z_i)}
\end{aligned}$$

### A.3.2 Further derivatives for Laplace approximations

For efficient calculations of the derivatives of log-determinants with STE, note that  $\frac{\partial \log \det(\Sigma^{-1} + Z^T W Z)}{\partial F_i} = \frac{\partial \log \det(\Sigma^{-1} + Z^T W Z)}{\partial \mu_i^*}$  and  $\frac{\partial \log \det(\Sigma^{-1} + Z^T W Z)}{\partial b_j^*} = \left( \frac{\partial \log \det(\Sigma^{-1} + Z^T W Z)}{\partial \mu^*} \right)^T \frac{\partial \mu^*}{\partial b_j^*} = \left( \frac{\partial \log \det(\Sigma^{-1} + Z^T W Z)}{\partial \mu^*} \right)^T Z_j$ . Therefore, we present in the following calculations for  $\frac{\partial \log \det(\Sigma^{-1} + Z^T W Z)}{\partial \mu_i^*}$ , and  $\frac{\partial \log \det(\Sigma^{-1} + Z^T W Z)}{\partial \xi_l}$  is obtained by replacing  $\frac{\partial W}{\partial \mu_i^*} = \text{diag}(-\frac{\partial^3 \log p(y_i | \mu_i^*, \xi)}{\partial \mu_i^{*3}})$  with  $\frac{\partial W}{\partial \xi_l} = \text{diag}(-\frac{\partial^3 \log p(y_i | \mu_i^*, \xi)}{\partial \mu_i^{*2} \partial \xi_l})$ . Further,  $\frac{\partial D}{\partial \mu_i^*}$  is a diagonal matrix with diagonal entries  $\left( \frac{\partial D}{\partial \mu_i^*} \right)_{ii} = \left( Z^T \frac{\partial W}{\partial \mu_i^*} Z \right)_{ii}$ , and  $\frac{\partial(L+D)}{\partial \mu_i^*}$  is a lower-triangular matrix with entries  $\left( \frac{\partial(L+D)}{\partial \mu_i^*} \right)_{ij} = \mathbf{1}_{\{i > j\}} \left( Z^T \frac{\partial W}{\partial \mu_i^*} Z \right)_{ij}$ .

$$\frac{\partial \log \det(\Sigma^{-1} + Z^T W Z)}{\partial \mu_i^*} \approx c \underbrace{\frac{\partial \log \det(P_{\text{SSOR}})}{\partial \mu_i^*}}_{\text{deterministic}} + \frac{\partial \log \det(\Sigma^{-1} + Z^T W Z)}{\partial \mu_i^*} - c \underbrace{\frac{\partial \log \det(P_{\text{SSOR}})}{\partial \mu_i^*}}_{\text{stochastic}}$$

$$\begin{aligned}
\underbrace{\frac{\partial \log \det(P_{\text{SSOR}})}{\partial \mu_i^*}}_{\text{deterministic}} &= \frac{\partial (\log \det(L + D) + \log \det(D^{-1}) + \log \det(L + D))}{\partial \mu_i^*} \\
&= \frac{\partial \log \det(D)}{\partial \mu_i^*} \\
&= \text{tr} \left( D^{-1} \frac{\partial D}{\partial \mu_i^*} \right)
\end{aligned}$$

$$\begin{aligned}
\frac{\partial \log \det(\Sigma^{-1} + Z^T W Z)}{\partial \mu_i^*} &= \text{tr} \left( (\Sigma^{-1} + Z^T W Z)^{-1} \frac{\partial(\Sigma^{-1} + Z^T W Z)}{\partial \mu_i^*} \right) \\
&= \text{tr} \left( (\Sigma^{-1} + Z^T W Z)^{-1} Z^T \frac{\partial W}{\partial \mu_i^*} Z \right) \\
&\approx \frac{1}{t} \sum_{i=1}^t \underbrace{((\Sigma^{-1} + Z^T W Z)^{-1} z_i)^T Z^T \frac{\partial W}{\partial \mu_i^*} Z P_{\text{SSOR}}^{-1} z_i}_{=: h(z_i)}
\end{aligned}$$

$$\begin{aligned}
\underbrace{\frac{\partial \log \det(P_{\text{SSOR}})}{\partial \mu_i^*}}_{\text{stochastic}} &= \text{tr} \left( P_{\text{SSOR}}^{-1} \frac{\partial P_{\text{SSOR}}}{\partial \mu_i^*} \right) \\
&= \text{tr} \left( P_{\text{SSOR}}^{-1} \frac{\partial(L + D) D^{-1} (L + D)^T}{\partial \mu_i^*} \right) \\
&= \text{tr} \left( P_{\text{SSOR}}^{-1} \left( 2 \frac{\partial(L + D)}{\partial \mu_i^*} D^{-1} (L + D)^T - (L + D) D^{-1} \frac{\partial D}{\partial \mu_i^*} D^{-1} (L + D)^T \right) \right) \\
&\approx \frac{1}{t} \sum_{i=1}^t \underbrace{\left( P_{\text{SSOR}}^{-1} z_i \right)^T \left( 2 \frac{\partial(L + D)}{\partial \mu_i^*} D^{-1} (L + D)^T - (L + D) D^{-1} \frac{\partial D}{\partial \mu_i^*} D^{-1} (L + D)^T \right) P_{\text{SSOR}}^{-1} z_i}_{=: r(z_i)}
\end{aligned}$$

#### A.4 Alternative stochastic trace estimation for Fisher information

For  $1 \leq k, l \leq K$  and  $z_i \sim \mathcal{N}(0, P)$ , the trace terms of the Fisher information in (7) can alternatively be computed with STE as follows:

$$\begin{aligned}
&\text{tr} \left( \Psi^{-1} \frac{\partial \Psi}{\partial \theta_k} \Psi^{-1} \frac{\partial \Psi}{\partial \theta_l} \right) \\
&= \text{tr} \left( (W - W Z (\Sigma^{-1} + Z^T W Z)^{-1} Z^T W) Z_k Z_k^T \right. \\
&\quad \left. (W - W Z (\Sigma^{-1} + Z^T W Z)^{-1} Z^T W) Z_l Z_l^T \right) \\
&= \text{tr} \left( W Z_k Z_k^T W Z_l Z_l^T \right) \\
&\quad - 2 \text{tr} \left( (\Sigma^{-1} + Z^T W Z)^{-1} Z^T W Z_k Z_k^T W Z_l Z_l^T Z W \right) \\
&\quad + \text{tr} \left( (\Sigma^{-1} + Z^T W Z)^{-1} Z^T W Z_k Z_k^T W Z (\Sigma^{-1} + Z^T W Z)^{-1} Z^T W Z_l Z_l^T Z W \right) \tag{54} \\
&\approx \text{tr} \left( W Z_k Z_k^T W Z_l Z_l^T \right) \\
&\quad - 2 \frac{1}{t} \sum_{i=1}^t \left( (\Sigma^{-1} + Z^T W Z)^{-1} z_i \right)^T Z^T W Z_k Z_k^T W Z_l Z_l^T Z W P^{-1} z_i \\
&\quad + \frac{1}{t} \sum_{i=1}^t \left( (\Sigma^{-1} + Z^T W Z)^{-1} z_i \right)^T Z^T W Z_k Z_k^T W Z (\Sigma^{-1} + Z^T W Z)^{-1} Z^T W Z_l Z_l^T Z W P^{-1} z_i.
\end{aligned}$$

## A.5 Preconditioned conjugate gradient algorithm

---

**Algorithm 4** Preconditioned conjugate gradient algorithm with Lanczos tridiagonal matrix

---

**Input:** Matrix  $A$ , preconditioner matrix  $P$ , vector  $b$

**Output:**  $u_{l+1} \approx A^{-1}b$ , tridiagonal matrix  $\tilde{T}$

```

1: early-stopping  $\leftarrow$  false
2:  $\alpha_0 \leftarrow 1$ 
3:  $\beta_0 \leftarrow 0$ 
4:  $u_0 \leftarrow 0$ 
5:  $r_0 \leftarrow b - Au_0$ 
6:  $z_0 \leftarrow P^{-1}r_0$ 
7:  $h_0 \leftarrow z_0$ 
8: for  $l \leftarrow 0$  to  $L$  do
9:    $v_l \leftarrow Ah_l$ 
10:   $\alpha_{l+1} \leftarrow \frac{r_l^T z_l}{h_l^T v_l}$ 
11:   $u_{l+1} \leftarrow u_l + \alpha_{l+1}h_l$ 
12:   $r_{l+1} \leftarrow r_l - \alpha_{l+1}v_l$ 
13:  if  $\|r_{l+1}\|_2 < \text{tolerance}$  then
14:    early-stopping  $\leftarrow$  true
15:  end if
16:   $z_{l+1} \leftarrow P^{-1}r_{l+1}$ 
17:   $\beta_{l+1} \leftarrow \frac{r_{l+1}^T z_{l+1}}{r_l^T z_l}$ 
18:   $h_{l+1} \leftarrow z_{l+1} + \beta_{l+1}h_l$ 
19:   $\tilde{T}_{l+1,l+1} \leftarrow \frac{1}{\alpha_{l+1}} + \frac{\beta_l}{\alpha_l}$ 
20:  if  $l > 0$  then
21:     $\tilde{T}_{l,l+1}, \tilde{T}_{l+1,l} \leftarrow \frac{\sqrt{\beta_l}}{\alpha_l}$ 
22:  end if
23:  if early-stopping then
24:    return  $u_{l+1}, \tilde{T}$ 
25:  end if
26: end for

```

---

## A.6 Zero fill-in incomplete Cholesky factorization

---

**Algorithm 5** Zero fill-in incomplete Cholesky algorithm

---

**Input:** Matrix  $A \in \mathbb{R}^{m \times m}$ , matrix  $S \in \mathbb{R}^{m \times m}$  with sparsity pattern

**Output:** Sparse lower triangular matrix  $L$  with  $A \approx LL^T$

```

1: for  $i \leftarrow 1$  to  $m$  do
2:   for  $j \leftarrow 1$  to  $m$  do
3:     if  $(i, j) \in S$  and  $i \geq j$  then
4:        $s \leftarrow L_{i \cdot} L_j^T$ 
5:       if  $i == j$  then
6:          $L_{ii} \leftarrow \sqrt{A_{ii} - s}$ 
7:       else
8:          $L_{ij} \leftarrow \frac{A_{ij} - s}{L_{jj}}$ 
9:       end if
10:      end if
11:    end for
12:  end for

```

---

## A.7 Simulating unbalanced random effects designs

The unbalanced designs are obtained as follows. We first generate numbers of repeated occurrences  $N_{jk}$  ( $=\sum_{i=1}^n (Z_k)_{ij}$ ) of random effect  $b_{k,j}$  for level  $j$  of component  $k$  by simulating from a negative binomial distribution with mean  $n/m_k - 1$  and size parameter  $r$  and then adding 1. The choice ensures that every random effect  $b_{k,j}$  occurs at least once, and there is variability in the numbers of repeated occurrences  $N_{jk}$ . Note that the size, or inverse overdispersion, parameter  $r$  control the regularity of the random effects design with smaller  $r$ 's yielding less regular designs with more variability in the number of occurrences per random effect. Unless stated otherwise, we use a size parameter  $r = 1$ . The resulting total numbers of occurrences  $T_k = \sum_{j=1}^{m_k} N_{jk}$  are typically close to  $n$ , but not exactly equal. Furthermore, the simulated totals  $T_1$  and  $T_2$  for the two random effect components usually differ slightly. To ensure that both components have the same total number of occurrences, we adjust the smaller of the two totals. If, say, the simulated total number of occurrences of the first component is smaller than that of the second component,  $T_1 < T_2$ , we add  $T_2 - T_1$  occurrences to the first component by simulating  $T_2 - T_1$  samples from a multinomial distribution with  $m_1$  factors and probabilities  $1/m_1$  and adding the resulting count vector to  $(N_{1,1}, \dots, N_{m_1,1})$ . Once the final values  $N_{jk}$  are obtained, we construct the incidence matrices  $Z_k$  by assigning exactly  $N_{jk}$  ones to column  $j$  in consecutive rows:

$$(Z_k)_{ij} = 1 \quad \text{for } i = \left( \sum_{j'=1}^{j-1} N_{j'k} \right) + 1, \dots, \sum_{j'=1}^j N_{j'k},$$

and zero otherwise (we use the convention  $\sum_{j'=1}^0 N_{j'k} = 0$ ). Finally, we randomly permute the rows of  $Z_2$ , which induces a random crossing structure between the two random effect components.

## A.8 Additional results for preconditioner comparison

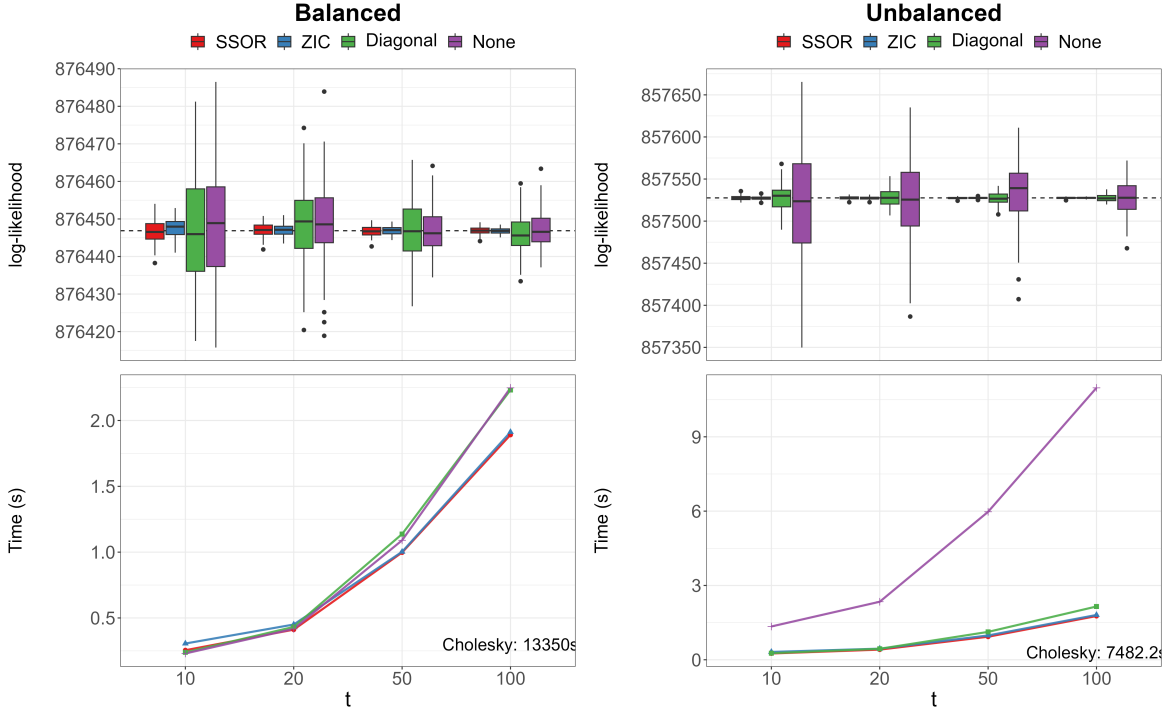


Figure 8: Negative log-likelihood and wall-clock time in seconds for different preconditioners and varying numbers of random vectors  $t$  in the SLQ method for a Gaussian likelihood. The dashed line represents the result for the Cholesky decomposition.

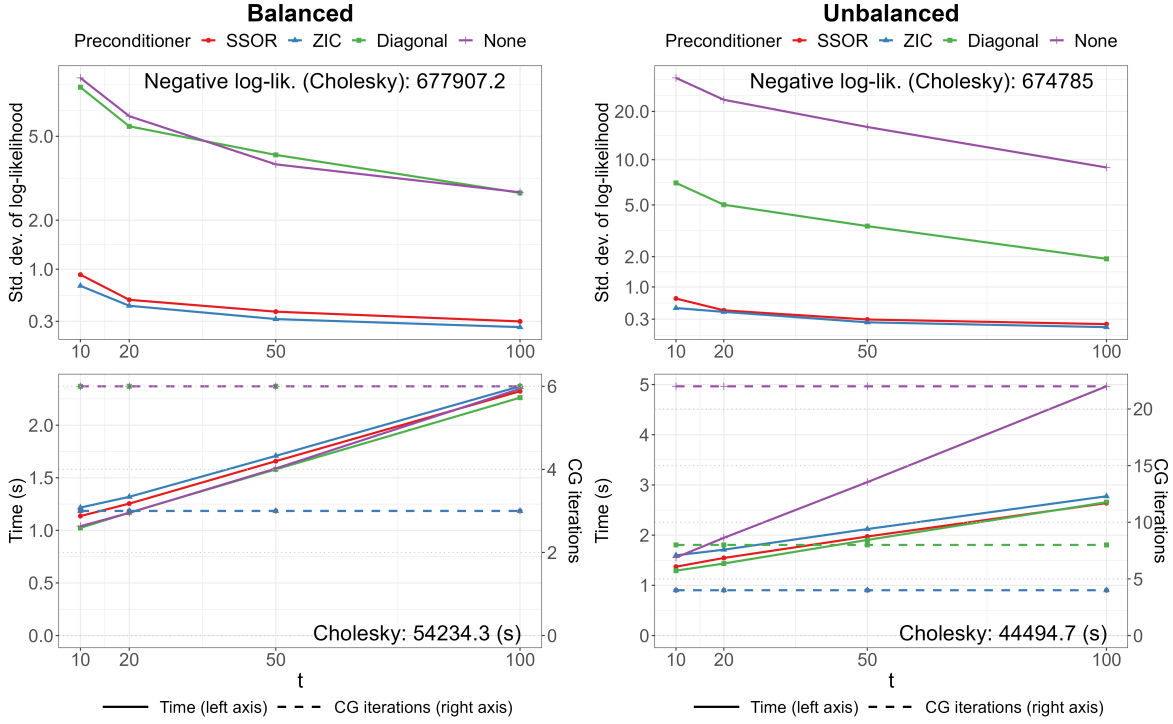


Figure 9: Accuracy (in standard deviations; top row), wall-clock time (in seconds; bottom row, left axis), and number of CG iterations (bottom row, right axis) for varying numbers of random vectors  $t$  in the SLQ method for calculating log-marginal likelihoods for a Bernoulli likelihood with a logit link.

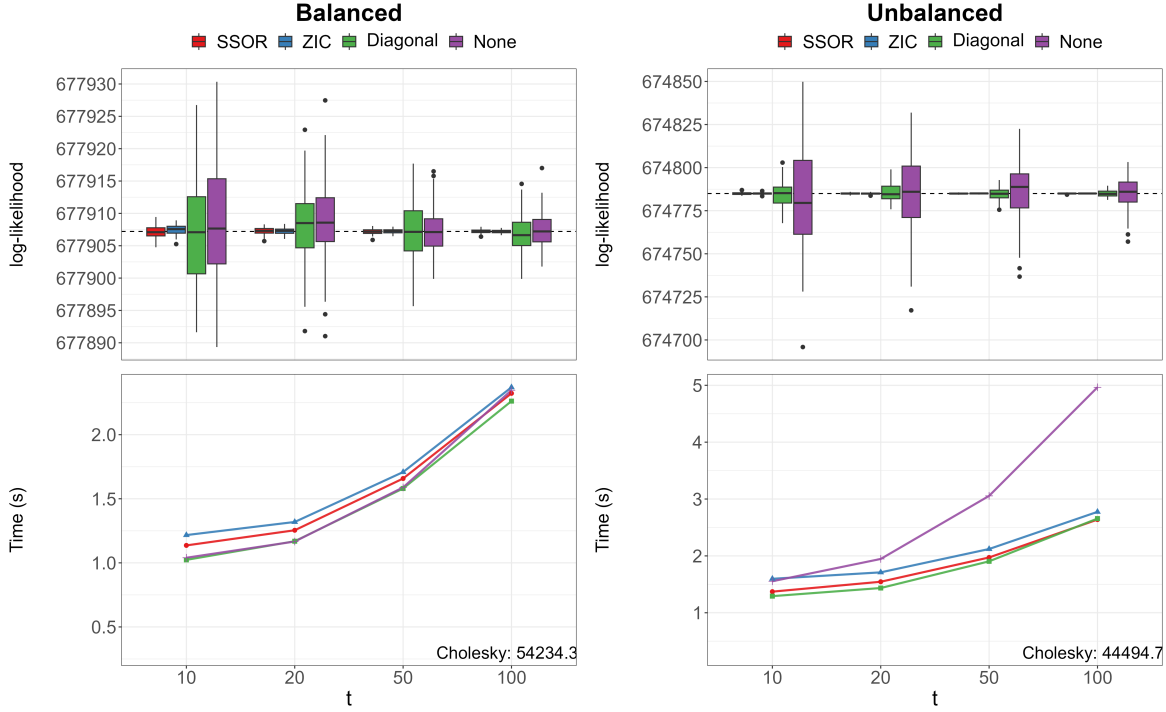


Figure 10: Negative log-likelihood and wall-clock time in seconds for varying numbers of random vectors  $t$  in the SLQ method for a Bernoulli likelihood with a logit link. The dashed line represents the result for the Cholesky decomposition.

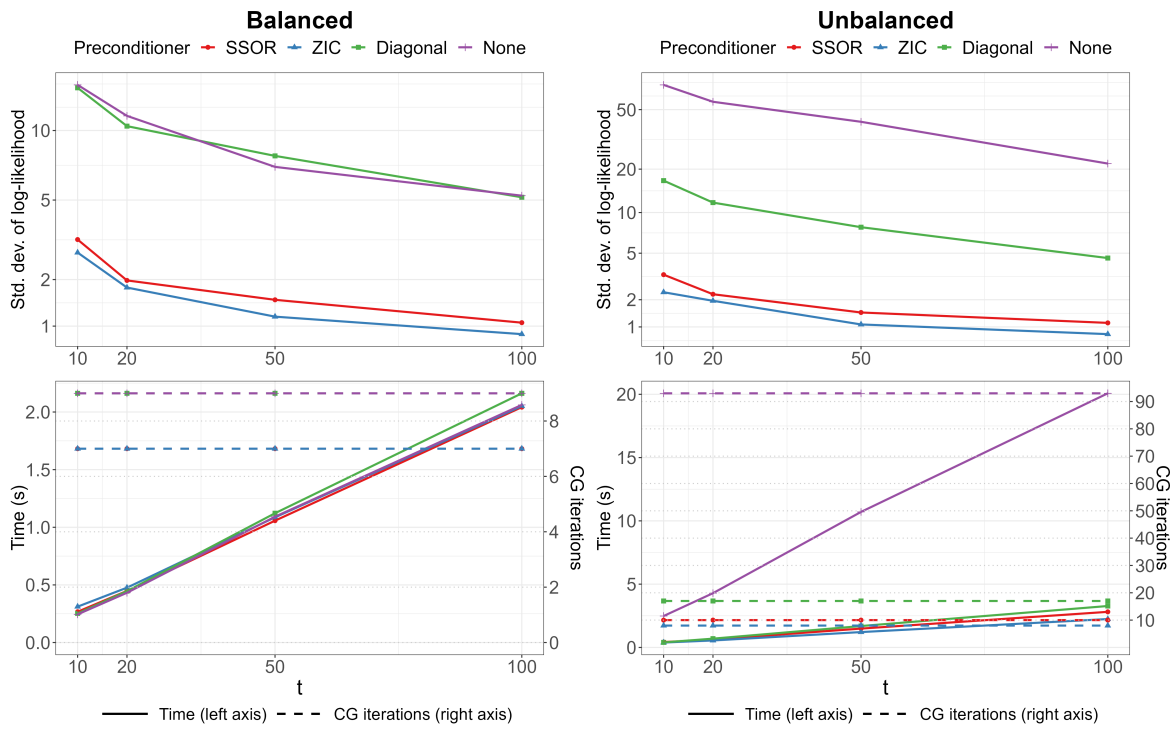


Figure 11: Accuracy (in standard deviations; top row), wall-clock time (in seconds; bottom row, left axis), and number of CG iterations (bottom row, right axis) for varying numbers of random vectors  $t$  in the SLQ method for calculating log-marginal likelihoods for a Gaussian likelihood with an error variance  $\sigma^2 = 0.05$  (= higher signal-to-noise ratio).

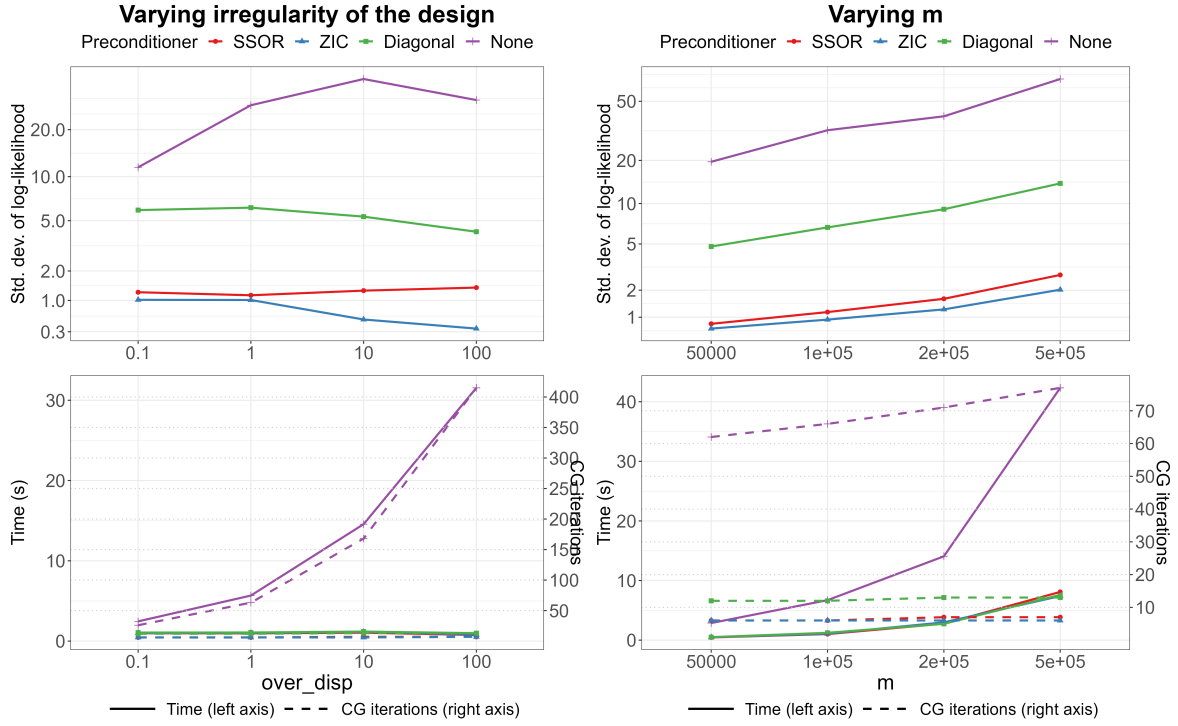


Figure 12: Accuracy (in standard deviations; top row), wall-clock time (in seconds; bottom row, left axis), and number of CG iterations (bottom row, right axis) for varying irregularity of the random effects design (left column) and random effects dimension  $m$  (right column) for calculating log-marginal likelihoods for a Gaussian likelihood. ‘over\_disp’ equals the inverse size parameter  $1/r$  in the unbalanced design simulation approach explained in Appendix A.7. A larger ‘over\_disp’ value corresponds to a less regular random effects design with more occurrences per random effect. An unbalanced design with  $r = 1$  is used when varying  $m$ .

## A.9 Additional results for parameter estimation and prediction in simulated experiments

	Krylov (GPBoost)	Cholesky (GPBoost)	lme4	glmmTMB
RMSE $\sigma^2$	$1.75 \times 10^{-3}$	$1.75 \times 10^{-3}$	$1.73 \times 10^{-3}$	$1.73 \times 10^{-3}$
Bias $\sigma^2$	$1.24 \times 10^{-4}$	$1.26 \times 10^{-4}$	$1.23 \times 10^{-4}$	$1.23 \times 10^{-4}$
RMSE $\sigma_1^2$	$8.97 \times 10^{-3}$	$8.96 \times 10^{-3}$	$8.83 \times 10^{-3}$	$8.83 \times 10^{-3}$
Bias $\sigma_1^2$	$-5.96 \times 10^{-4}$	$-6.15 \times 10^{-4}$	$-5.57 \times 10^{-4}$	$-5.57 \times 10^{-4}$
RMSE $\sigma_2^2$	$8.34 \times 10^{-3}$	$8.35 \times 10^{-3}$	$8.13 \times 10^{-3}$	$8.13 \times 10^{-3}$
Bias $\sigma_2^2$	$1.79 \times 10^{-4}$	$1.56 \times 10^{-4}$	$1.53 \times 10^{-4}$	$1.54 \times 10^{-4}$
RMSE $\beta_0$	$1.46 \times 10^{-2}$	$1.46 \times 10^{-2}$	$1.46 \times 10^{-2}$	$1.46 \times 10^{-2}$
Bias $\beta_0$	$1.36 \times 10^{-3}$	$1.36 \times 10^{-3}$	$1.36 \times 10^{-3}$	$1.36 \times 10^{-3}$
RMSE $\beta_1$	$1.17 \times 10^{-2}$	$1.17 \times 10^{-2}$	$1.17 \times 10^{-2}$	$1.17 \times 10^{-2}$
Bias $\beta_1$	$-2.06 \times 10^{-4}$	$-2.06 \times 10^{-4}$	$-2.06 \times 10^{-4}$	$-2.06 \times 10^{-4}$
RMSE $\beta_2$	$1.08 \times 10^{-2}$	$1.08 \times 10^{-2}$	$1.08 \times 10^{-2}$	$1.08 \times 10^{-2}$
Bias $\beta_2$	$-4.41 \times 10^{-4}$	$-4.41 \times 10^{-4}$	$-4.41 \times 10^{-4}$	$-4.41 \times 10^{-4}$
RMSE $\beta_3$	$1.25 \times 10^{-2}$	$1.25 \times 10^{-2}$	$1.25 \times 10^{-2}$	$1.25 \times 10^{-2}$
Bias $\beta_3$	$-1.14 \times 10^{-3}$	$-1.14 \times 10^{-3}$	$-1.14 \times 10^{-3}$	$-1.14 \times 10^{-3}$
RMSE $\beta_4$	$1.31 \times 10^{-2}$	$1.31 \times 10^{-2}$	$1.31 \times 10^{-2}$	$1.31 \times 10^{-2}$
Bias $\beta_4$	$1.28 \times 10^{-3}$	$1.28 \times 10^{-3}$	$1.28 \times 10^{-3}$	$1.28 \times 10^{-3}$
RMSE $\beta_5$	$1.06 \times 10^{-2}$	$1.06 \times 10^{-2}$	$1.06 \times 10^{-2}$	$1.06 \times 10^{-2}$
Bias $\beta_5$	$3.21 \times 10^{-4}$	$3.21 \times 10^{-4}$	$3.21 \times 10^{-4}$	$3.21 \times 10^{-4}$

Table 2: Root mean squared error (RMSE) and bias of the variance and coefficient estimates for Gaussian likelihoods.

	Krylov (GPBoost)	Cholesky (GPBoost)	glmmTMB
RMSE $\sigma_1^2$	$2.01 \times 10^{-2}$	$2.01 \times 10^{-2}$	$2.05 \times 10^{-2}$
Bias $\sigma_1^2$	$-1.15 \times 10^{-2}$	$-1.15 \times 10^{-2}$	$-1.13 \times 10^{-2}$
RMSE $\sigma_2^2$	$2.15 \times 10^{-2}$	$2.15 \times 10^{-2}$	$2.20 \times 10^{-2}$
Bias $\sigma_2^2$	$-1.36 \times 10^{-2}$	$-1.36 \times 10^{-2}$	$-1.36 \times 10^{-2}$
RMSE $\beta_0$	$1.73 \times 10^{-2}$	$1.73 \times 10^{-2}$	$1.73 \times 10^{-2}$
Bias $\beta_0$	$-3.68 \times 10^{-4}$	$-3.67 \times 10^{-4}$	$-4.76 \times 10^{-4}$
RMSE $\beta_1$	$5.18 \times 10^{-2}$	$5.18 \times 10^{-2}$	$5.10 \times 10^{-2}$
Bias $\beta_1$	$1.33 \times 10^{-3}$	$1.34 \times 10^{-3}$	$7.09 \times 10^{-4}$
RMSE $\beta_2$	$5.33 \times 10^{-2}$	$5.33 \times 10^{-2}$	$5.19 \times 10^{-2}$
Bias $\beta_2$	$-6.51 \times 10^{-3}$	$-6.53 \times 10^{-3}$	$-5.87 \times 10^{-3}$
RMSE $\beta_3$	$5.10 \times 10^{-2}$	$5.09 \times 10^{-2}$	$5.05 \times 10^{-2}$
Bias $\beta_3$	$6.00 \times 10^{-4}$	$5.82 \times 10^{-4}$	$1.86 \times 10^{-4}$
RMSE $\beta_4$	$5.25 \times 10^{-2}$	$5.25 \times 10^{-2}$	$5.24 \times 10^{-2}$
Bias $\beta_4$	$-1.24 \times 10^{-3}$	$-1.23 \times 10^{-3}$	$-1.30 \times 10^{-3}$
RMSE $\beta_5$	$5.18 \times 10^{-2}$	$5.18 \times 10^{-2}$	$4.99 \times 10^{-2}$
Bias $\beta_5$	$-6.36 \times 10^{-3}$	$-6.36 \times 10^{-3}$	$-5.61 \times 10^{-3}$

Table 3: Root mean squared error (RMSE) and bias of the variance and coefficient estimates for Bernoulli likelihoods.

	Krylov (GPBoost)	Cholesky (GPBoost)	lme4	glmmTMB
RMSE	$1.62 \times 10^{-1}$	$1.62 \times 10^{-1}$	$1.62 \times 10^{-1}$	$1.62 \times 10^{-1}$
sd(RMSE)	$2.32 \times 10^{-4}$	$2.32 \times 10^{-4}$	$2.32 \times 10^{-4}$	$2.32 \times 10^{-4}$
LS	$-4.01 \times 10^{-1}$	$-4.01 \times 10^{-1}$		
sd(LS)	$1.40 \times 10^{-3}$	$1.40 \times 10^{-3}$		

Table 4: Average root mean squared error (RMSE) for predictive means and average log score (LS) for probabilistic predictions with corresponding standard errors for Gaussian likelihoods.

	Krylov (GPBoost)	Cholesky (GPBoost)	glmmTMB
RMSE	$5.00 \times 10^{-1}$	$5.00 \times 10^{-1}$	$5.00 \times 10^{-1}$
sd(RMSE)	$5.37 \times 10^{-4}$	$5.37 \times 10^{-4}$	$5.37 \times 10^{-4}$
LS	$7.26 \times 10^{-1}$	$7.26 \times 10^{-1}$	
sd(LS)	$1.12 \times 10^{-3}$	$1.12 \times 10^{-3}$	

Table 5: Average root mean squared error (RMSE) for predictive means and average log score (LS) for probabilistic predictions with corresponding standard errors for Bernoulli likelihoods.

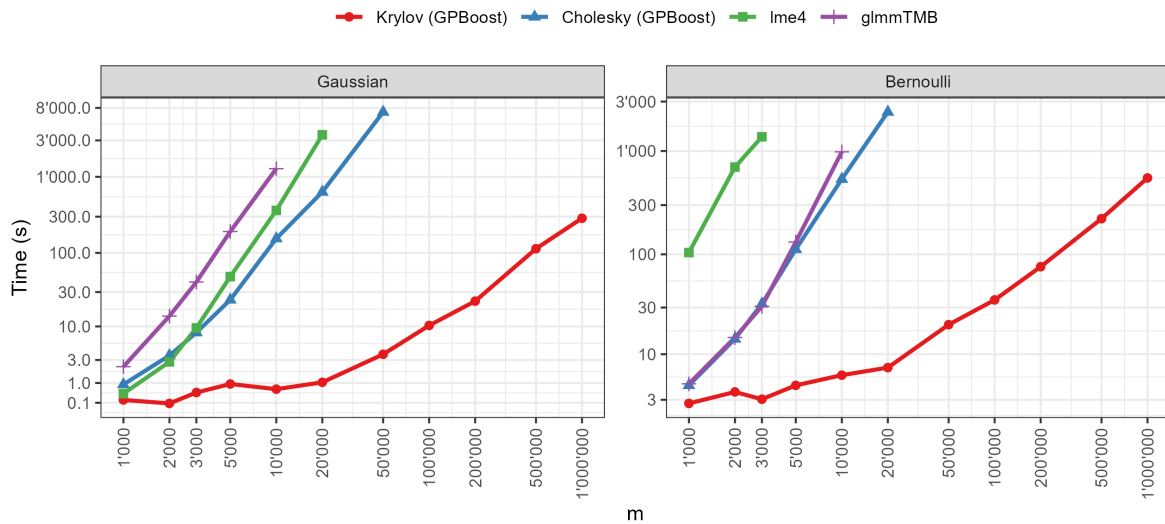


Figure 13: Average wall clock times (s) for parameter estimation and different  $m$  with  $m_2 = \frac{m_1}{2}$ . The dimensions of the random effects  $m$  are chosen so that they are divisible by three and correspond as closely as possible to those in Figure 3. Simulated data follows either a Gaussian or a Bernoulli likelihood.

## A.10 Additional results for the real-world applications

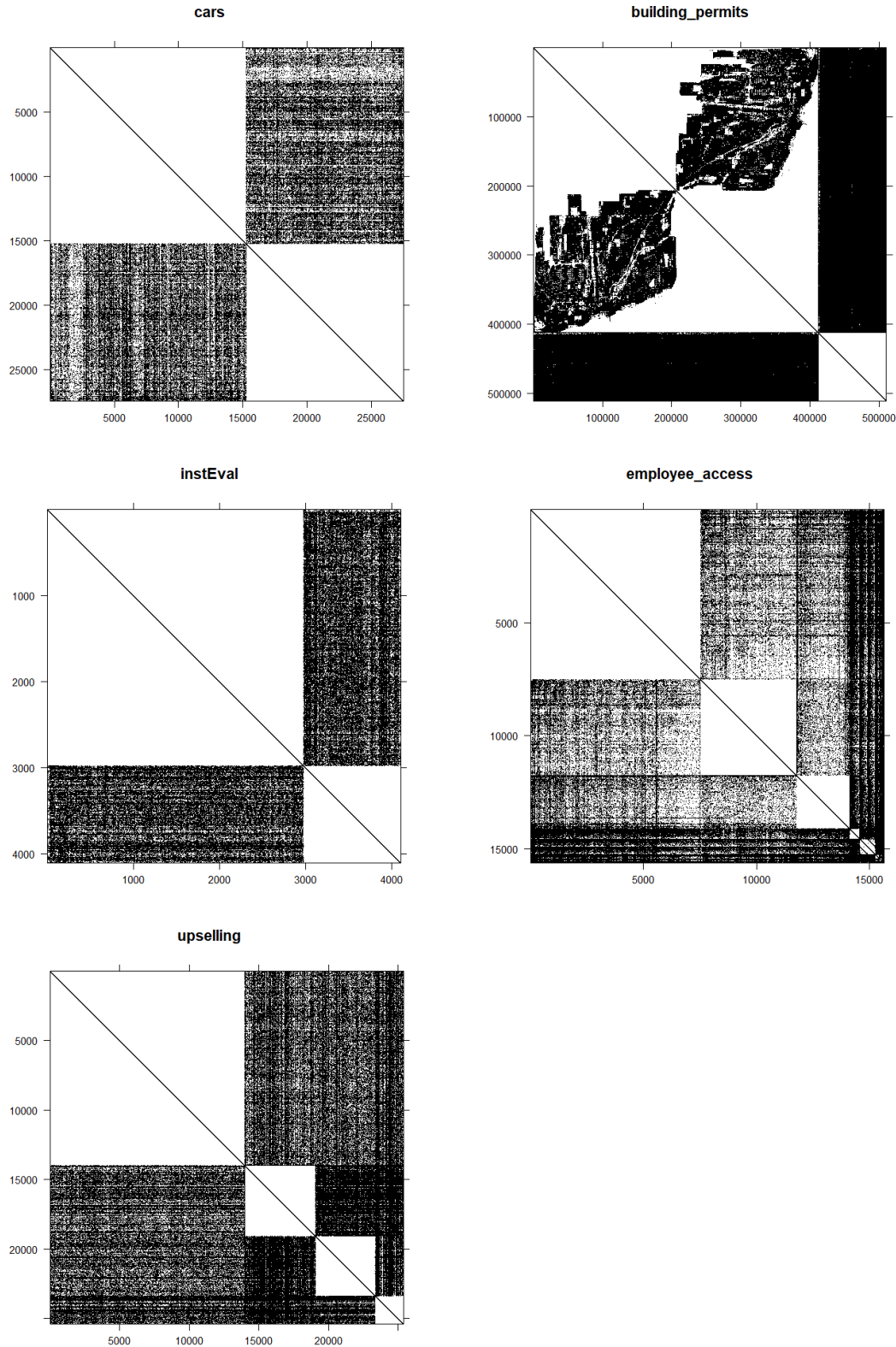


Figure 14: Non-zero entries of the matrix  $Z^T Z$  for the real-world data sets (except the MovieLens\_32m data set for which  $Z^T Z$  is too large to visualize).

data set	method	Time (s)	nll_optimum
cars	Cholesky (GPBoost)	104.3	27518.0
	Krylov (GPBoost)	7.7	27517.1
	glmmTMB	1152.2	27518.1
	lme4	62.3	27518.0
building_permits	Cholesky (GPBoost)	5647.5	867567.7
	Krylov (GPBoost)	97.4	867566.5
	glmmTMB	3763.2	867567.8
	lme4	600.0	867567.3
instEval	Cholesky (GPBoost)	9.4	118764.0
	Krylov (GPBoost)	0.5	118763.5
	glmmTMB	76.1	118764.0
	lme4	11.5	118764.0
MovieLens_32m	Cholesky (GPBoost)	crashed	
	Krylov (GPBoost)	283.8	40613057
	glmmTMB	crashed	
	lme4	273152.9	40613057
employee_access	Cholesky (GPBoost)	628.0	5494.4
	Krylov (GPBoost)	80.5	5492.3
	glmmTMB	287.9	5494.4
	lme4	8362.9	5504.5
upselling	Cholesky (GPBoost)	1747.8	11488.5
	Krylov (GPBoost)	41.1	11488.4
	glmmTMB	crashed	
	lme4	crashed	

Table 6: Time for parameter estimation and negative log-marginal likelihood at the optimum for different real-world data sets and models.

data set	method	$\sigma^2$	$\sigma_1^2$	$\sigma_2^2$	$\sigma_3^2$
cars	Cholesky (GPBoost)	$5.24 \times 10^{-2}$	$3.28 \times 10^{-1}$	$2.04 \times 10^{-1}$	
	Krylov (GPBoost)	$5.24 \times 10^{-2}$	$3.28 \times 10^{-1}$	$2.04 \times 10^{-1}$	
	glmmTMB	$5.24 \times 10^{-2}$	$3.28 \times 10^{-1}$	$2.04 \times 10^{-1}$	
	lme4	$5.24 \times 10^{-2}$	$3.28 \times 10^{-1}$	$2.04 \times 10^{-1}$	
building_permits	Cholesky (GPBoost)	$1.31 \times 10^0$	$9.10 \times 10^{-1}$	$3.98 \times 10^{-2}$	$3.97 \times 10^{-2}$
	Krylov (GPBoost)	$1.31 \times 10^0$	$9.09 \times 10^{-1}$	$3.98 \times 10^{-2}$	$3.96 \times 10^{-2}$
	glmmTMB	$1.31 \times 10^0$	$9.10 \times 10^{-1}$	$3.69 \times 10^{-2}$	$4.25 \times 10^{-2}$
	lme4	$1.31 \times 10^0$	$9.10 \times 10^{-1}$	$7.93 \times 10^{-2}$	$1.08 \times 10^{-4}$
instEval	Cholesky (GPBoost)	$1.38 \times 10^0$	$1.07 \times 10^{-1}$	$2.57 \times 10^{-1}$	
	Krylov (GPBoost)	$1.38 \times 10^0$	$1.07 \times 10^{-1}$	$2.57 \times 10^{-1}$	
	glmmTMB	$1.38 \times 10^0$	$1.07 \times 10^{-1}$	$2.57 \times 10^{-1}$	
	lme4	$1.38 \times 10^0$	$1.07 \times 10^{-1}$	$2.57 \times 10^{-1}$	
MovieLens_32m	Cholesky (GPBoost)	crashed			
	Krylov (GPBoost)	$7.23 \times 10^{-1}$	$1.93 \times 10^{-1}$	$2.32 \times 10^{-1}$	
	glmmTMB	crashed			
	lme4	$7.23 \times 10^{-1}$	$1.93 \times 10^{-1}$	$2.32 \times 10^{-1}$	
employee_access	Cholesky (GPBoost)		$1.52 \times 10^0$	$5.78 \times 10^0$	$9.48 \times 10^{-6}$
	Krylov (GPBoost)		$1.52 \times 10^0$	$5.79 \times 10^0$	$1.17 \times 10^{-5}$
	glmmTMB		$1.52 \times 10^0$	$5.78 \times 10^0$	$3.14 \times 10^{-10}$
	lme4		$1.60 \times 10^0$	$6.06 \times 10^0$	$0.00 \times 10^0$
upselling	Cholesky (GPBoost)		$3.56 \times 10^{-1}$	$2.59 \times 10^{-1}$	$9.86 \times 10^{-3}$
	Krylov (GPBoost)		$3.58 \times 10^{-1}$	$2.58 \times 10^{-1}$	$9.58 \times 10^{-3}$
	glmmTMB	crashed			
	lme4	crashed			

Table 7: Estimates for  $\sigma^2$ ,  $\sigma_1^2$ ,  $\sigma_2^2$ , and  $\sigma_3^2$  for different real-world data sets and models. For reasons of space, we do not report estimates for other variance parameters.

data set	method	$\beta_0$	$\beta_1$	$\beta_2$	$\beta_3$
cars	Cholesky (GPBoost)	$1.02 \times 10^1$	$3.50 \times 10^{-1}$	$-1.77 \times 10^{-1}$	$-2.64 \times 10^{-3}$
	Krylov (GPBoost)	$1.02 \times 10^1$	$3.50 \times 10^{-1}$	$-1.77 \times 10^{-1}$	$-2.64 \times 10^{-3}$
	glmmTMB	$1.02 \times 10^1$	$3.50 \times 10^{-1}$	$-1.77 \times 10^{-1}$	$-2.63 \times 10^{-3}$
	lme4	$1.02 \times 10^1$	$3.50 \times 10^{-1}$	$-1.77 \times 10^{-1}$	$-2.64 \times 10^{-3}$
building_permits	Cholesky (GPBoost)	$3.62 \times 10^0$	$5.44 \times 10^{-4}$	$-1.36 \times 10^{-5}$	$2.01 \times 10^{-3}$
	Krylov (GPBoost)	$3.62 \times 10^0$	$5.44 \times 10^{-4}$	$-1.36 \times 10^{-5}$	$2.00 \times 10^{-3}$
	glmmTMB	$3.62 \times 10^0$	$5.44 \times 10^{-4}$	$-1.36 \times 10^{-5}$	$2.02 \times 10^{-3}$
	lme4	$3.62 \times 10^0$	$5.44 \times 10^{-4}$	$-1.36 \times 10^{-5}$	$2.01 \times 10^{-3}$
instEval	Cholesky (GPBoost)	$3.31 \times 10^0$	$5.21 \times 10^{-2}$	$7.23 \times 10^{-2}$	$1.37 \times 10^{-1}$
	Krylov (GPBoost)	$3.31 \times 10^0$	$5.21 \times 10^{-2}$	$7.23 \times 10^{-2}$	$1.37 \times 10^{-1}$
	glmmTMB	$3.31 \times 10^0$	$5.21 \times 10^{-2}$	$7.23 \times 10^{-2}$	$1.37 \times 10^{-1}$
	lme4	$3.31 \times 10^0$	$5.21 \times 10^{-2}$	$7.23 \times 10^{-2}$	$1.37 \times 10^{-1}$
MovieLens_32m	Cholesky (GPBoost)	crashed			
	Krylov (GPBoost)	$3.39 \times 10^0$	$-7.29 \times 10^{-2}$	$-4.93 \times 10^{-2}$	
	glmmTMB	crashed			
	lme4	$3.39 \times 10^0$	$-7.29 \times 10^{-2}$	$-4.93 \times 10^{-2}$	
employee_access	Cholesky (GPBoost)	$7.21 \times 10^0$			
	Krylov (GPBoost)	$7.16 \times 10^0$			
	glmmTMB	$7.19 \times 10^0$			
	lme4	$6.92 \times 10^0$			
upselling	Cholesky (GPBoost)	$-1.74 \times 10^0$	$2.32 \times 10^{-5}$	$9.42 \times 10^{-3}$	$3.86 \times 10^{-6}$
	Krylov (GPBoost)	$-1.74 \times 10^0$	$2.32 \times 10^{-5}$	$9.48 \times 10^{-3}$	$3.94 \times 10^{-6}$
	glmmTMB	crashed			
	lme4	crashed			

Table 8: Estimates for  $\beta_0$ ,  $\beta_1$ ,  $\beta_2$ , and  $\beta_3$  for different real-world data sets and models. For reasons of space, we do not report estimates for other coefficients.